

## Upregulation of MG53 Induces Diabetic Cardiomyopathy Through Transcriptional Activation of Peroxisome Proliferation-Activated Receptor $\alpha$

Fenghua Liu, PhD\*; Ruisheng Song, PhD\*; Yuanqing Feng, BS\*; Jiaojiao Guo, BS; Yanmin Chen, BS; Yong Zhang, BS; Tao Chen, BS; Yanru Wang, BS; Yanyi Huang, PhD; Chuan-Yun Li, PhD; Chunmei Cao, MD, PhD; Yan Zhang, MD, PhD; Xinli Hu, PhD; Rui-ping Xiao, MD, PhD

**Background**—Diabetic cardiomyopathy, which contributes to >50% diabetic death, is featured by myocardial lipid accumulation, hypertrophy, fibrosis, and cardiac dysfunction. The mechanism underlying diabetic cardiomyopathy is poorly understood. Recent studies have shown that a striated muscle-specific E3 ligase Mitsugumin 53 (MG53, or TRIM72) constitutes a primary causal factor of systemic insulin resistance and metabolic disorders. Although it is most abundantly expressed in myocardium, the biological and pathological roles of MG53 in triggering cardiac metabolic disorders remain elusive.

**Methods and Results**—Here we show that cardiac-specific transgenic expression of MG53 induces diabetic cardiomyopathy in mice. Specifically, MG53 transgenic mouse develops severe diabetic cardiomyopathy at 20 weeks of age, as manifested by insulin resistance, compromised glucose uptake, increased lipid accumulation, myocardial hypertrophy, fibrosis, and cardiac dysfunction. Overexpression of MG53 leads to insulin resistant via destabilizing insulin receptor and insulin receptor substrate 1. More importantly, we identified a novel role of MG53 in transcriptional upregulation of peroxisome proliferation-activated receptor alpha and its target genes, resulting in lipid accumulation and lipid toxicity, thereby contributing to diabetic cardiomyopathy.

**Conclusions**—Our results suggest that overexpression of myocardial MG53 is sufficient to induce diabetic cardiomyopathy via dual mechanisms involving upregulation of peroxisome proliferation-activated receptor alpha and impairment of insulin signaling. These findings not only reveal a novel function of MG53 in regulating cardiac peroxisome proliferation-activated receptor alpha gene expression and lipid metabolism, but also underscore MG53 as an important therapeutic target for diabetes mellitus and associated cardiomyopathy. (*Circulation*. 2015;131:795-804. DOI: 10.1161/CIRCULATIONAHA.114.012285.)

**Key Words:** diabetic cardiomyopathies ■ insulin resistance ■ MG53 protein, mouse ■ peroxisome proliferation-activated receptors

Diabetes mellitus is an emerging global threat to human health. It is estimated that the total number of people experiencing diabetes mellitus will reach 366 million in 2030.<sup>1</sup> Although hypertension and coronary narrowing are major pathogenic factors of acquired cardiomyopathy, diabetes mellitus has been established as an independent risk factor since 1972.<sup>2</sup> Diabetic cardiomyopathy, as a major complication, is the leading cause of morbidity and mortality for diabetic patients. Epidemiological studies have demonstrated that diabetic people have a 2- to 5-fold increase of risk in developing heart failure compared with age-matched healthy subjects

after adjusting for age, blood pressure, weight, cholesterol level, and coronary artery disease.<sup>3-7</sup>

### Editorial see p 771 Clinical Perspective on p 804

Rodent models are of particular value in study of diabetic cardiomyopathy because there is minimal confounding involvement of coronary atherosclerosis. It has been demonstrated that diabetic mice and rats fed with high-fat diet display cardiac remodeling and dysfunction.<sup>8-11</sup> Recently we and others have shown that mice overexpressing Mitsugumin 53 (MG53)

Received July 15, 2014; accepted December 29, 2014.

From Institute of Molecular Medicine (F.L., R.S., Y.F., J.G., Y.Z., Y.W., C.L., C.C., Y.Z., X.H., R.X.), State Key Laboratory of Biomembrane and Membrane Biotechnology (F.L., R.S., Y.F., J.G., Y.C., Y.Z., Y.W., C.C., Y.Z., X.H., R.X.), Biodynamic Optical Imaging Center (T.C., Y.H.), Center for Life Sciences (Y.C., C.L., R.X.), and Beijing City Key Laboratory of Cardiometabolic Molecular Medicine (R.X.), Peking University, Beijing, China.

\*Drs Liu and Song and Y. Feng contributed equally to this study.

Current address for R.S.: Department of Biological Chemistry and Molecular Pharmacology, Harvard Medical School, Boston, MA.

The online-only Data Supplement is available with this article at <http://circ.ahajournals.org/lookup/suppl/doi:10.1161/CIRCULATIONAHA.114.012285/-/DC1>.

Correspondence to Rui-Ping Xiao, MD, PhD or Xinli Hu, PhD, Institute of Molecular Medicine, Peking University, 5 Yiheyuan Road, Beijing 100871, China. E-mail [xiaor@pku.edu.cn](mailto:xiaor@pku.edu.cn) or [huxxx025@pku.edu.cn](mailto:huxxx025@pku.edu.cn)

© 2015 American Heart Association, Inc.

*Circulation* is available at <http://circ.ahajournals.org>

DOI: 10.1161/CIRCULATIONAHA.114.012285

develop obesity, systemic insulin resistance, dyslipidemia, and hyperglycemia, whereas MG53 deficiency prevents high-fat diet-induced metabolic disorders, including obesity, dyslipidemia, and hyperglycemia.<sup>12,13</sup> MG53 was originally shown to play an important role in membrane repair.<sup>14,15</sup> We have shown that MG53 acts as an E3 ligase targeting insulin receptor (IR) and insulin receptor substrate 1 (IRS1) for ubiquitin-dependent degradation, resulting in insulin resistance and metabolic disorders.<sup>12</sup> However, it is possible that MG53 regulates not only insulin-dependent glucose metabolism but also lipid metabolism. In addition, we and others have reported that MG53 is abundantly expressed in the heart as well as skeletal muscle and involved in ischemia-mediated cardiac preconditioning and postconditioning.<sup>16,17</sup> But it is unclear whether MG53 plays a role in the regulation of myocardial glucose and lipid metabolism. In particular, we seek to determine the potential function of MG53 in regulating myocardial lipid metabolism and its malfunction in the pathogenesis of diabetic cardiomyopathy.

To understand the exact role of MG53 in the myocardial metabolism, in this study we have generated transgenic mice with cardiac-specific overexpression of MG53 (MG53 h-TG) via alpha myosin heavy chain ( $\alpha$ -MHC) promoter. The MG53 h-TG mice developed typical diabetic cardiomyopathy symptoms characterized by myocardial insulin resistance, defective substrate utilization, cardiac fibrosis, ventricular hypertrophy, and cardiac dysfunction. Mechanistically, in addition to the compromised insulin signaling, the expression levels of peroxisome proliferation-activated receptor alpha (PPAR- $\alpha$ ) and its downstream target genes were markedly increased in the MG53 h-TG hearts, but downregulated in the MG53-deficient hearts. These findings suggest that MG53 contributes to the pathogenesis of diabetic cardiomyopathy via, at least in part, activation of PPAR- $\alpha$  signaling pathway.

## Material and Methods

### Animals

All animal procedures were carried out in compliance with the protocols approved by the Institute of Animal Care and Use Committee of Peking University, and in accordance with the *Guide for the Care and Use of Laboratory Animals* (National Institutes of Health publication No. 86-23, revised 1985).

### Generation of the MG53 h-TG mice

The MG53 transgenic construct was generated by cloning the MG53cDNA into an expression vector containing the  $\alpha$ -MHC promoter (a gift from Dr Jeff Robbins, the Heart Institute, Department of Pediatrics, The Cincinnati Children's Hospital Medical Center, OH). The MG53 h-TG construct was injected into 1-cell embryos of C57BL/6 mice. The transgenic founders were further crossed with C57BL/6. Age-matched male mice of MG53 h-TG and their wild-type littermates (WT, C57BL/6) were used in this study.

### Echocardiography

Mice were anesthetized with 4% chloral hydrate (1 mL/100g body weight), and echocardiography assessment was performed using a VEVO-2100 machine (Visual Sonics) with an M-mode Doppler.

### In Vitro Palmitate Uptake Assay

Neonatal rat ventricular myocytes (NRVMs) were infected with Ad-MG53-GFP or Ad-MG53-Myc virus 24 h before palmitate

stimulation. Cells in the control groups were infected with Ad-GFP or Ad- $\beta$ -gal, respectively. Before images were obtained, NRVMs were incubated in DMEM with 2% BSA with or without 100  $\mu$ mol/L palmitate for 6 h. Then, lipid uptake was determined using a stimulated Raman scattering system.<sup>18,19</sup>

### In Vitro Glucose Uptake Assay

Male adult rat ventricular myocytes infected with either Adv-GFP or Adv-MG53-GFP were incubated with Krebs-Ringer phosphate buffer (128 mmol/L NaCl, 1.4 mmol/L CaCl<sub>2</sub>, 1.4 mmol/L MgSO<sub>4</sub>, 5.2 mmol/L KCl, and 10 mmol/L Na<sub>2</sub>HPO<sub>4</sub>, pH7.4) containing glucose (3 mmol/L), and then treated with 100 nmol/L insulin for 30 minutes at 37°C, and exposed to 2-[1,2-<sup>3</sup>H]-deoxy-D-glucose (1  $\mu$ Ci/mL, 0.02  $\mu$ mol/L) for the final 5 minutes. Then, the cells were washed 3 times with ice-cold PBS and solubilized with 0.5 mol/L NaOH. The cell associated radioactivity was determined by scintillation counting. Nonspecific counts, determined in the presence of 20  $\mu$ mol/L cytochalasin B, were subtracted from each value as previously described.<sup>20</sup>

### Real-Time Polymerase Chain Reaction

Total RNA was isolated with Trizol reagent (Invitrogen) and 2  $\mu$ g was reverse-transcribed into cDNA using RT-MLV reverse transcriptase (Promega). The RT reaction mixture was used as template to perform real-time polymerase chain reaction (PCR; Stepone Plus Real-Time PCR System, Applied Biosystems). The relative mRNA levels were determined by normalizing to the 18S rRNA level. The primers used are listed in Table I in the online-only Data Supplement.

### Small-Interfering RNA

NRVMs were transfected with small-interfering RNA (siRNA; RiboBio Co. Ltd.) specifically targeting PPAR- $\alpha$  using Lipofectamine RNAi MAX (Invitrogen) according to the manufacturer's instructions. The sequences of siRNAs against PPAR- $\alpha$  are listed in Table II in the online-only Data Supplement.

### RNA-Seq

Total RNA was extracted from MG53 h-TG or WT mice. RNA-Seq libraries were prepared from 4 hearts from each group. Next-generation sequencing was performed on an Illumina HiSeq2000 sequencing system according to the manufacturer's instructions. RNA-Seq reads were mapped to the mouse genome (version mm9) by TopHat (version v2.0.8), according to computational pipelines as reported previously.<sup>21</sup> Tools such as DAVID<sup>22,23</sup> and Qiagen's Ingenuity Pathway Analysis (IPA, QIAGEN Redwood City, www.qiagen.com/ingenuity) were used for functional enrichment analyses and pathway network analyses, respectively.

### ChIP-PCR

ChIP assay was conducted using a chromatin immunoprecipitation (ChIP) kit (Millipore). The procedure was performed following the protocol provided by the manufacturer. Primers used for ChIP-PCR are listed in Table III in the online-only Data Supplement.

### Statistical Analysis

Data are presented as mean $\pm$ SEM. Statistical analysis was performed with prism 5.0 or SPSS 17.0. Data sets were tested for normality of distribution with Kolmogorov-Smirnov tests. Data groups with normal distribution were compared using unpaired Student *t* test. The Mann-Whitney *U* test was used for nonparametric data. Comparisons between multiple groups were assessed by 1-way ANOVA with Bonferroni post hoc analysis. For the oxygen consumption experiment, repeated measures ANOVA was used to compare the oxygen consumption rate between the WT and MG53 h-TG cardiac myocytes over the time course. A *P*<0.05 was considered as significant.

More information of methods could be found in the online-only Data Supplement.

## Results

### MG53 h-TG Mice Display Symptoms of Diabetic Cardiomyopathy

Two lines of MG53 h-TG mice were generated by overexpressing MG53 driven by the  $\alpha$ -MHC promoter (Figure 1A and 1B in the online-only Data Supplement). At 20 weeks of age, the body weight of the MG53 h-TG mice was not significantly different from their WT littermates. However, hearts from both lines of MG53 h-TG mice were overtly enlarged with ventricular dilation and cardiac dysfunction. In this study, we opted to use the first line of MG53 h-TG mice for detailed phenotyping and mechanistic studies. Specifically, the inter-ventricular inner diameter and the weight of the MG53 h-TG hearts were increased by 22% and 15%, respectively, compared with WT (Figure 1A and 1B). Myocardial hypertrophy was also evidenced by increased ratio of heart weight to tibia length (Figure 1C) and hypertrophic gene expression profile, including inversed changes of  $\alpha$ -MHC and  $\beta$ -MHC expression and upregulation of atrial natriuretic peptide and brain natriuretic peptide (Figure 1D). In addition, MG53 h-TG hearts had augmented lipid deposition as compared with WT (Figure 1E, upper panel, and Figure 1IA in the online-only Data Supplement). Myocardial fibrosis was detected in the MG53 h-TG but not WT hearts (Figure 1E, lower panel, and Figure 1IIB in the online-only Data Supplement). Enhanced fibrosis in the MG53 h-TG hearts would decrease ventricular compliance, which is a major pathogenic process

of maladaptive cardiac structure remodeling and functional insufficiency. Indeed, cardiac cross sections and ECHO measurements revealed ventricular dilation and cardiac dysfunction as manifested by enlarged left ventricular inner diameter with reduced posterior wall thickness and significantly suppressed ejection fraction and fractional shortening (Figure 1F and 1G, and Table IV in the online-only Data Supplement). Thus, cardiac-specific overexpression of MG53 is sufficient to recapitulate the phenotype of diabetic cardiomyopathy.

### MG53 Overexpression Causes Cardiac Insulin Resistance

In our previous study, globally overexpressing MG53 leads to an obese phenotype resembling *db/db* mice, featured by impaired insulin signaling, obesity, dyslipidemia, and hyperglycemia.<sup>12</sup> We and others have demonstrated that MG53 binds to the IR and IRS1 and subsequently mediates ubiquitin-dependent degradation of IR and IRS1 through its E3 ligase activity.<sup>12,13,24</sup> Consistent with these previous reports, we found that IR and IRS1 protein levels were reduced by  $\approx 40\%$  in the MG53 h-TG hearts relative to WT controls (Figure 2A). Because IR and IRS1 sense and respond to insulin stimulation, their degradation would be expected to cause deterioration in insulin signaling. Indeed, insulin signaling was markedly impaired in the hearts from MG53 h-TG mice as manifested by diminished myocardial Akt phosphorylation in response to insulin stimulation (Figure 2B). To obtain mechanistic insight in a defined in vitro setting, we overexpressed GFP-tagged

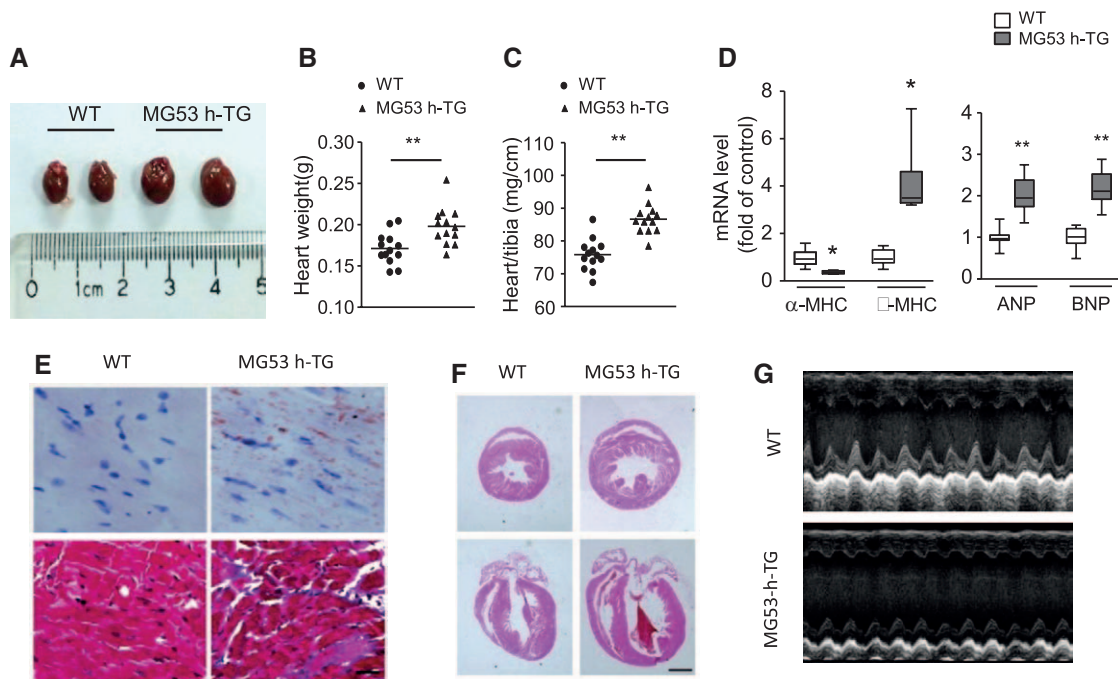


**Figure 1.** Cardiac-specific overexpression of MG53 leads to cardiomyopathy. **A**, Transgenic mice with cardiac-specific overexpression of MG53 (MG53 h-TG) hearts were enlarged. **B** and **C**, The heart weight (**B**) and the ratio of heart weight to tibia length (**C**) were significantly increased in the MG53 h-TG mice. **D**, The mRNA levels of  $\alpha$ -myosin heavy chain (MHC),  $\beta$ -MHC, atrial natriuretic peptide (ANP), and brain natriuretic peptide (BNP) of MG53 h-TG hearts relative to wild-type (WT) controls. **E**, Oil red O staining revealed increased neutral triglyceride deposition in the heart from MG53 h-TG mice (**top**). Fibrosis of the hearts from the 2 groups was assessed by Masson staining (**bottom**). **F**, The gross morphology of MG53 h-TG hearts showing the ventricular dimensions and ventricular wall thickness by sections along the shorter (**top**) and longer (**bottom**) axes of the heart. **G**, Representative echocardiographic images of the left ventricle showing ventricular dilation and cardiac dysfunction. Scale bar in **F**, 1 mm; in **E**, 20  $\mu$ m. Data in **B**, **C**, and **D** are mean $\pm$ SEM (\* $P$ <0.05, \*\* $P$ <0.01 vs WT control; n=8–10 for each group).

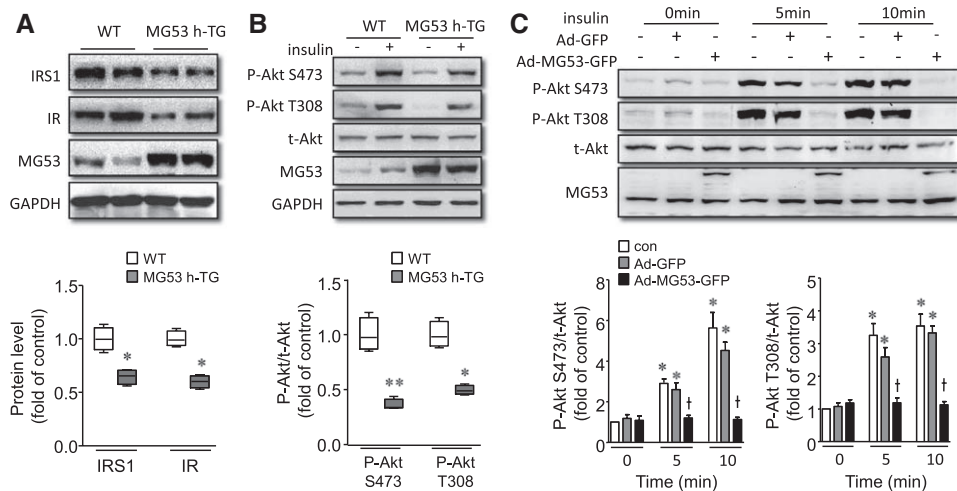


**Figure 2.** MG53 overexpression causes reduced protein abundance of insulin receptor (IR) and insulin receptor substrate 1 (IRS1) and impaired insulin signaling in the heart. **A**, The protein abundance of IR and IRS1 in wild-type (WT) and transgenic mice with cardiac-specific overexpression of MG53 (MG53 h-TG). **B**, The insulin-induced phosphorylation of Akt was attenuated in the MG53 h-TG mouse heart. **C**, In adult rat ventricular myocytes (ARVMs), phosphorylation of Akt at sites S473 and T308 after insulin stimulation was robustly blocked by MG53 overexpression. Data are mean $\pm$ SEM (\* $P$ <0.05, \*\* $P$ <0.01 vs WT for **A** and **B**; in **C**, \* $P$ <0.05 vs 0 minutes [in the absence of insulin], † $P$ <0.05 vs Ad-GFP;  $n$ =3–4 for each group). Ad-GFP indicates cells infected with adenovirus expressing GFP; Ad-MG53-GFP, cells infected with adenovirus expressing MG53-GFP fusion protein; and con, control cells with no adenovirus infection.

MG53 in cultured adult rat ventricular myocytes using adenoviral gene transfer, and found that insulin-induced phosphorylation of Akt at both T308 and S473 was almost completely blocked by MG53 overexpression (Figure 2C). Because insulin signaling pathway is one of the major pathways regulating cellular energy metabolism,<sup>25,26</sup> induction of insulin resistance may be a pivotal event in causing metabolic derangement in hearts subjected to MG53 overexpression.

### MG53 Overexpression Alters Cardiac Nutrient Utilization

Physiologically, lipids contribute to  $\approx$ 70% of the energy supply for the working heart, whereas the rest is provided by glucose and lactate.<sup>27,28</sup> It has been implicated that the insulin-resistant heart becomes even more dependent on free fatty acids (FFA) for its energy needs,<sup>29</sup> and that diabetic cardiomyopathy is associated with this kind of shift in substrate preference.<sup>30,31</sup> To test whether MG53 is involved in the regulation of myocardial substrate use, we took the advantage of highly sensitive stimulated Raman scattering microscopy technology to detect FFA in situ. By detecting the unique vibrational signature of FFA, stimulated Raman scattering microscopy allows label-free visualization and quantitative analysis of lipids in living cells.<sup>18</sup> In NRVMs overexpressing MG53, uptake of palmitate was enhanced by about 3-fold (Figure 3A). In contrast, insulin-stimulated 2-[1,2-<sup>3</sup>H]-deoxy-D-glucose uptake by cardiomyocytes was completely abrogated (Figure 3B). These results suggest that MG53 overexpression decreases glucose uptake, but facilitates FFA uptake, tipping the myocardial substrate use further toward lipids. Because, relative to glucose, FFA requires more oxygen for its  $\beta$ -oxidation, the oxygen consumption rate is an indicator of substrate utilization by cells. Besides at the indicated time points where the oxygen consumption rate of the MG53 h-TG cardiomyocytes is significantly elevated, repeated measurements analysis showed that oxygen consumption rate of the MG53 h-TG

was significantly higher than that of the WT over the entire time course of measurement (Figure 3C), indicating that the MG53 h-TG heart consumes more FFA, even though its contractility was suppressed (Figure 1F and 1G, and Table IV in the online-only Data Supplement). Thus, the enhanced FFA uptake and use compromise cardiac function of MG53 h-TG mice, recapitulating the hallmark of increased myocardial oxygen consumption associated with reduced cardiac function in diabetic mice.<sup>32</sup>

### Pathways Relevant to Diabetic Cardiomyopathy Are Induced in the MG53 h-TG Mouse Heart

To delineate the mechanism underlying MG53-mediated alterations in myocardial energy substrate use, we analyzed genome-wide gene expression profile in the hearts from MG53 h-TG mice versus WT controls using RNA deep sequencing (RNA-Seq) approach. We selected 916 genes from the MG53 h-TG RNA-seq data set that fit the criteria of fragments per kilobases of exon per million fragments mapped (FPKM) $>$ 0.5 and  $P$ <0.05, and analyzed these genes using the online RNA deep sequencing analysis tool DAVID (Database for Annotation, Visualization and Integrated Discovery, <http://david.abcc.ncifcrf.gov/>). The pathways affected by MG53 overexpression are listed in Figure 4A. Among them, hypertrophic cardiomyopathy, dilated cardiomyopathy, and the PPAR- $\alpha$  signaling pathways were the most relevant to the cardiac phenotype in the MG53 h-TG mice, and interestingly they were all activated by MG53 overexpression (Figure 4B). In contrast, a mirrored gene expression profile was found in the RNA-Seq data obtained from MG53 knockout (MG53 KO) mouse heart (Figure IIIA and IIIB in the online-only Data Supplement). To test whether genes involved in FFA metabolism were affected in MG53 h-TG mice, we selected several genes involved in lipid metabolism and examined their expression in the MG53 h-TG heart by real-time PCR. As expected, the mRNA levels of the most of these genes were up-regulated in the MG53 overexpressing

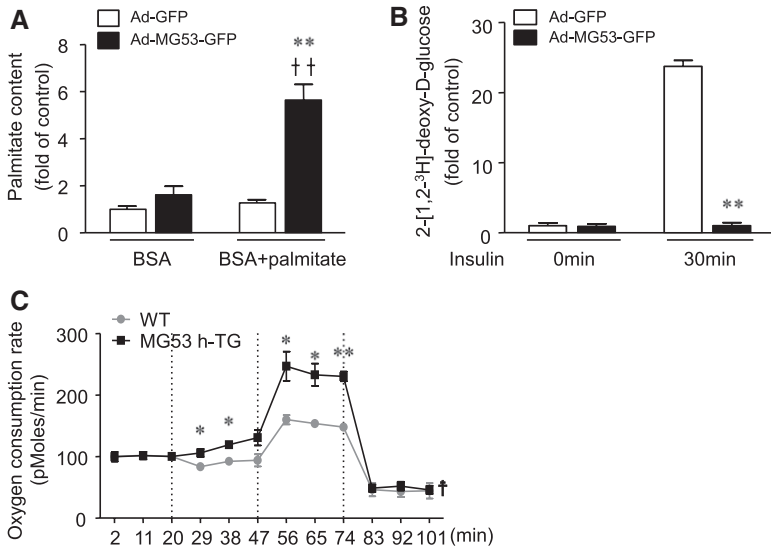


**Figure 3.** MG53 overexpression causes a glucose-free fatty acid (FFA) use shift and increased oxygen consumption rate (OCR). **A**, In neonatal rat ventricular myocytes (NRVMs), label-free images were obtained by stimulated Raman scattering (SRS) microscopy to determine the palmitate content in cells after 6 h of incubation with palmitate. **B**, In cultured adult rat ventricular myocytes (ARVMs), overexpression of MG53 by adenovirus infection inhibited insulin-mediated 2-[1,2-<sup>3</sup>H]-deoxy-D-glucose uptake. **C**, OCR analysis showed that cardiomyocytes isolated from mice with cardiac-specific overexpression of MG53 (MG53 h-TG) consumed more oxygen than those from wild-type (WT) mice. Data are mean $\pm$ SEM (\* $P$ <0.05, \*\* $P$ <0.01 vs Ad-GFP for **A** and **B**, vs WT control in **C**; †† $P$ <0.01 vs treated with BSA alone, ‡ $P$ <0.05 over the entire time course,  $n$ =3 for each group).

hearts (Figure 4C). Concomitantly, the genes promoting glycolysis were systematically suppressed, whereas the expression of pyruvate dehydrogenase kinase (PDK) 1 and 3, which inhibit the key enzyme pyruvate dehydrogenase (PDH) in glycolysis, were significantly upregulated (Figure 4D). Thus, in the MG53 h-TG heart, the lipid metabolism pathways are enhanced, whereas glycolysis is repressed. Importantly, PPAR- $\alpha$  pathway was activated in the MG53 h-TG hearts (Figure 4B), but repressed in the MG53 KO hearts (Figure IIIB in the online-only Data Supplement). Because PPAR- $\alpha$  is the key regulator of lipid metabolism, the dysregulation of PPAR- $\alpha$  would disturb myocardial lipid homeostasis.<sup>33,34</sup> The impaired PPAR- $\alpha$  pathway caused by alterations in MG53 expression led us to further examine the role of PPAR- $\alpha$  in the MG53 h-TG hearts.

**Upregulation of MG53 Is Associated With an Elevation of PPAR- $\alpha$  Expression in Various Animal Models of Metabolic Disorders**

Next, to determine whether PPAR- $\alpha$  is upregulated in the high-expressed MG53 contexts, we measured the protein abundance

of PPAR- $\alpha$  in MG53 h-TG mice and multiple metabolic disease models. In the MG53 overexpressing heart, the PPAR- $\alpha$  expression level was increased compared with WT controls (Figure 5A). In our previous study, we found that MG53 expression is increased in the skeletal muscle of *db/db* diabetic mice, high-fat diet-induced obese mice, and rhesus monkeys with spontaneous metabolic syndrome featured by obesity, dyslipidemia, and hyperglycemia.<sup>35</sup> Similarly, an upregulation of MG53 was also detected in the myocardium of these animal models (Figure 5B–5D). It is noteworthy that the elevation of myocardial MG53 protein level was universally accompanied by an increase in PPAR- $\alpha$  protein abundance in these metabolic disease models. Moreover, RNA-Seq data demonstrated that the mRNA levels of MG53 as well as PPAR- $\alpha$  in the heart (Figure IVA and IVB in the online-only Data Supplement) and the skeletal muscle (Figure IVC and IVD in the online-only Data Supplement) were increased in the mice fed with high-fat diet. These data indicate that the expression of MG53 is strongly linked with the expression level of PPAR- $\alpha$ , and that MG53 may participate in the transcriptional regulation of PPAR- $\alpha$ .

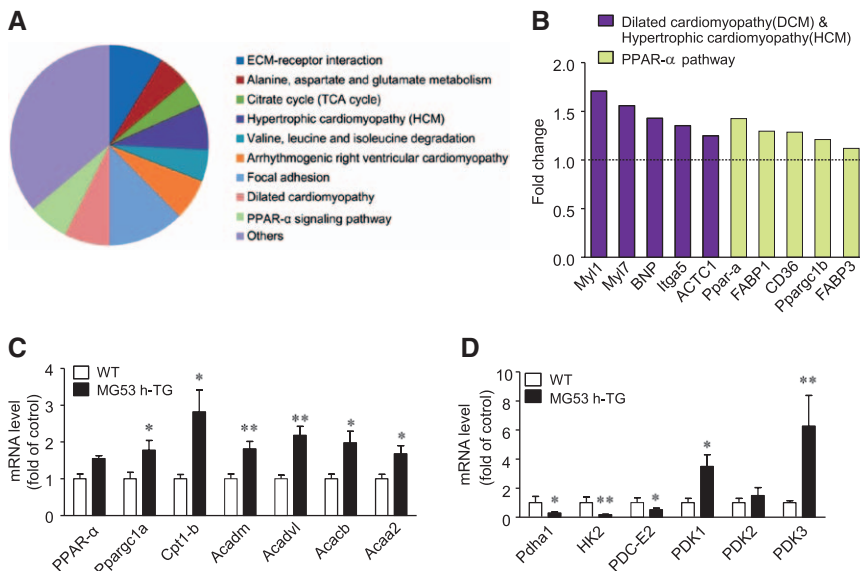


**Figure 4.** Pathways relevant to diabetic cardiomyopathy are induced in the heart of mice with cardiac-specific overexpression of MG53 (MG53 h-TG). **A**, Categories of genes influenced by MG53 overexpression according to Database for Annotation, Visualization, and Integrated Discovery analysis. **B**, Changes of the genes related to dilated cardiomyopathy, hypertrophic cardiomyopathy, and the peroxisome proliferation-activated receptor alpha (PPAR- $\alpha$ ) pathway. **C**, Real-time polymerase chain reaction (PCR) showed that the mRNA levels of genes involved in free fatty acid (FFA) metabolism were elevated in the MG53 h-TG heart compared with that in the wild-type (WT) mouse hearts. **D**, The mRNA levels genes involved in glucose metabolism in the hearts from WT or MG53 h-TG mice were assayed with real-time PCR. Data in **C** and **D** are plotted as mean $\pm$ SEM (\* $P$ <0.05, \*\* $P$ <0.01 vs WT control;  $n$ =8–10 for each group).

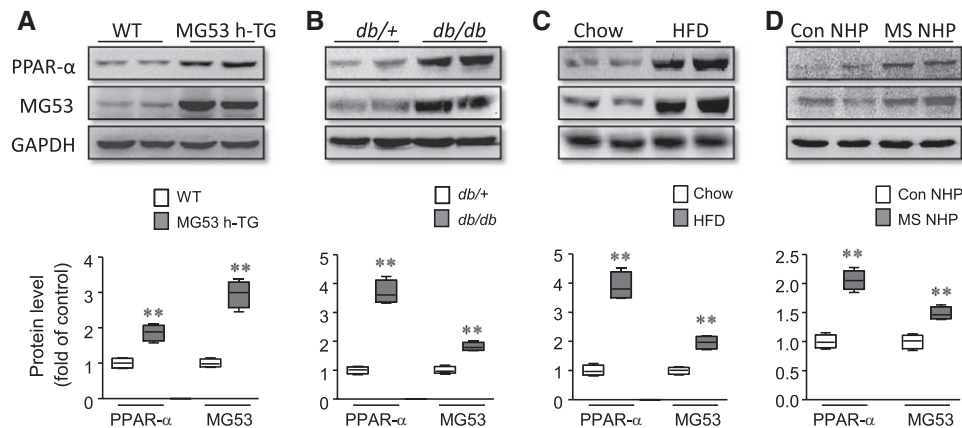


**Figure 5.** Accompanying increases in peroxisome proliferation-activated receptor alpha (PPAR- $\alpha$ ) and MG53 expression were detected in various animal models with metabolic disorders. **A**, In the heart of mice with cardiac-specific overexpression of MG53 (MG53 h-TG), PPAR- $\alpha$  was upregulated. **B–D**, In models of different metabolic disorders, *db/db* mice (**B**), high-fat diet (HFD)-fed mice (**C**), and a rhesus model with spontaneous metabolic disorder (**D**), the increase in PPAR- $\alpha$  expression level was associated with the augmentation of MG53 expression. Data are expressed as mean $\pm$ SEM (\*\* $P$ <0.05, \*\* $P$ <0.01 vs respective control;  $n$ =3–4).

### MG53 Regulates PPAR- $\alpha$ Expression at the Transcriptional Level

To further establish the relationship between the abundance of MG53 and the expression of PPAR- $\alpha$  we suppressed or enhanced MG53 expression in cultured cardiac myocytes by either shRNA-mediated gene knockdown or adenovirus-mediated gene transfer, respectively. Knocking down of MG53, indeed, markedly reduced PPAR- $\alpha$  mRNA and protein levels in NRVMs (Figure 6A, and Figure VA in the online-only Data Supplement). In contrast, adenovirus-mediated overexpression of MG53 led to a 2-fold increase in the expression of PPAR- $\alpha$  at both the mRNA and protein levels (Figure 6B and 6C). Thus, upregulation of MG53 is sufficient to increase PPAR- $\alpha$  expression at both mRNA and protein levels in cardiac myocytes.

MG53, also known as TRIM72, belongs to the tripartite motif (TRIM) family. A few members of the TRIM family can regulate gene transcription. To determine whether MG53 also participates in transcriptional regulation, we first examined the intracellular distribution of endogenous as well as GFP-tagged MG53 in cultured neonatal rat cardiomyocytes. Immunofluorescence staining revealed that MG53 was homogeneously distributed in the cytosol with an enrichment in the nuclear compartment in some of the cells (Figure 6D). This was corroborated by cytosolic/nuclear fraction analysis (Figure 6E). The enforced expression of GFP-tagged MG53 exhibited a global cellular distribution pattern with a nuclear enrichment in some of the cells (Figure VB in the online-only Data Supplement). Furthermore, the overexpressed MG53 in the MG53 h-TG hearts could be detected in both cytosolic and nuclear fraction (Figure VC in the online-only Data Supplement). Thus, the subcellular localization of MG53 suggests that it may elicit nuclear functions. To determine whether MG53 is directly involved in transcriptional regulation, we fused MG53 with the DNA binding domain (DBD) of Gal4 to tether MG53 to the Gal4-responsive promoter.<sup>36</sup> When this Gal4-MG53 fusion protein was cotransfected into H9c2 cells with the Gal4-responsive luciferase reporter construct, it induced reporter gene expression, whereas cotransfection of Flag-MG53 alone did not induce the reporter activity (Figure VD in the online-only Data

Supplement). This result indicates that MG53 can activate transcription when it is recruited to a target promoter.

We then constructed reporter constructs driven by the nested deletions of PPAR- $\alpha$  promoter. When MG53 was overexpressed, the reporter gene activity was significantly increased except the 150-bp construct, suggesting that MG53 enhances the promoter activity of PPAR- $\alpha$  (Figure 6F). To further ascertain that MG53 was recruited to the PPAR- $\alpha$  promoter, we performed ChIP assay in NRVMs with adenoviral gene transfer of MG53. Consistent with the reporter assay, the region between –140 and –2 of PPAR- $\alpha$  gene was enriched in the ChIP-PCR analysis (Figure 6G), suggesting that MG53 is recruited to this region of PPAR- $\alpha$  promoter.

### MG53 Promotes Palmitate Uptake via Enhancing the Expression of PPAR- $\alpha$ and Its Target Genes

Because PPAR- $\alpha$  is a pivotal regulator of lipid metabolism,<sup>33,34</sup> we further analyzed the PPAR network and found that the expression of many genes in this pathway were altered in the MG53 h-TG mouse heart (Figure VI in the online-only Data Supplement). Most importantly, overexpression of MG53 led to the upregulation of PPAR- $\alpha$  target genes, CD36 and FABP3, in the transgenic hearts. It has been shown that  $\approx$ 70% of the fatty acids transported into cells is mediated by CD36.<sup>37,38</sup> The mRNA and protein levels of CD36 and FABP3 were augmented in the MG53 h-TG hearts (Figure 7A–7C). This was not caused by cardiac compensation, because adenoviral gene transfer of MG53 was also able to profoundly increase gene expression of CD36 and FABP3 in the well-controlled settings of cultured adult and neonatal cardiomyocytes (Figure 7D and 7E), whereas shRNA-mediated MG53 gene silencing significantly suppressed the expression of both genes (Figure 7F). These results indicate that upregulation of PPAR- $\alpha$  key target genes, CD36 and FABP3, is essentially involved in MG53-mediated FFA uptake and utilization, as well as lipid accumulation in the myocardium.

Next, we determined whether upregulation of PPAR- $\alpha$  is obligated to MG53-mediated augmentation of FFA uptake. We first examined the effect of MG53 deficiency in lipid uptake. When the expression of MG53 was inhibited by specific shRNA in

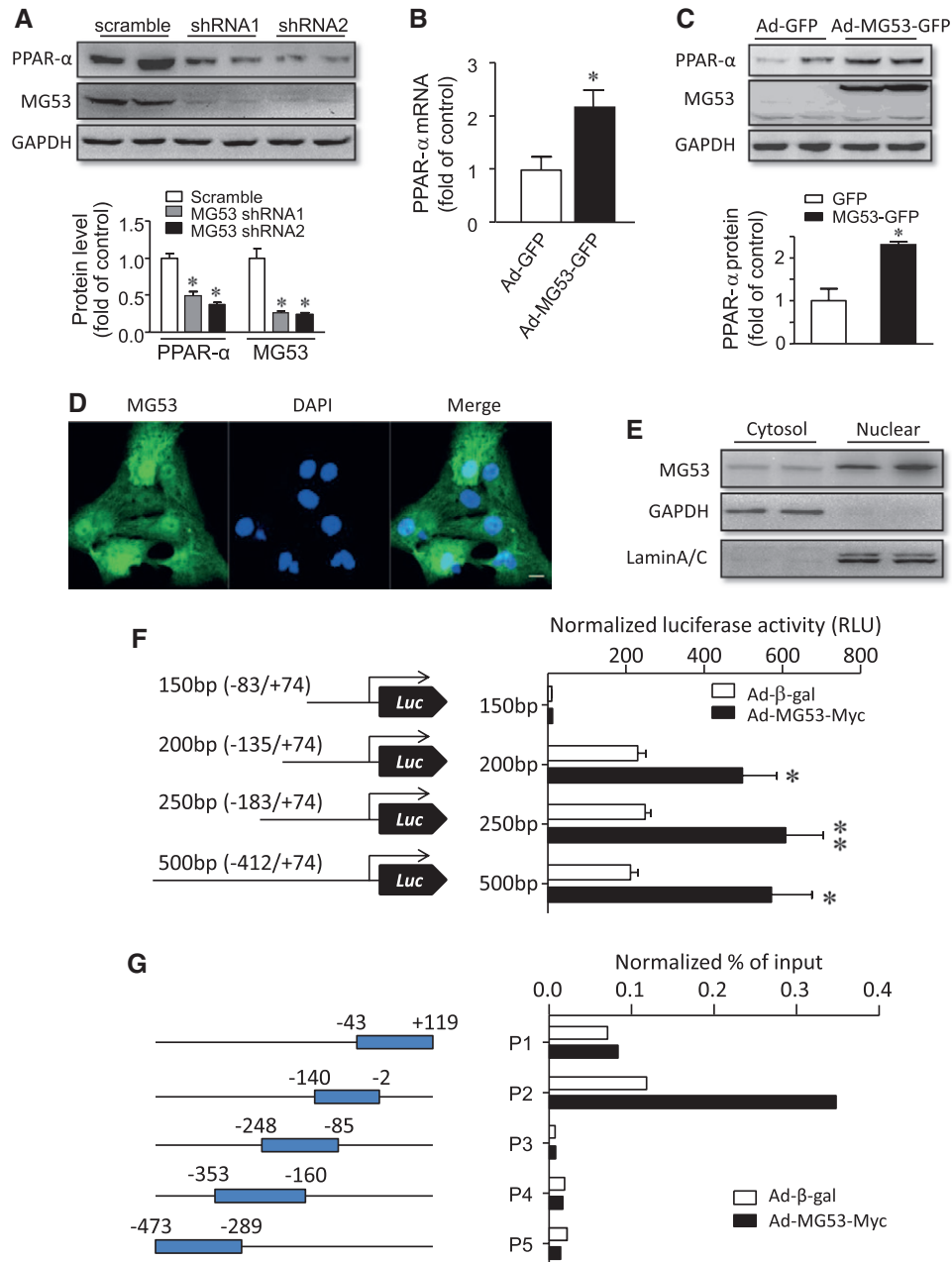


**Figure 6.** MG53 regulates peroxisome proliferation-activated receptor alpha (PPAR- $\alpha$ ) expression at the transcriptional level. **A**, The PPAR- $\alpha$  protein level was decreased when MG53 was knocked down by 2 effective shRNAs. **B**, Real-time polymerase chain reaction (PCR) showed an increase of PPAR- $\alpha$  expression in adult rat ventricular myocytes (ARVMs) overexpressing MG53. **C**, The PPAR- $\alpha$  protein level was increased by MG53 overexpression in ARVMs. **D**, Immuno-confocal staining showed the homogenous distribution of MG53 in neonatal rat ventricular myocytes (NRVMs). **E**, Western blots of the cytosolic and nuclear fractions of NRVMs demonstrated that MG53 was present in both the cytosol and nucleus. Similar results were obtained in 3 independent experiments. **F**, The activity of luciferase reporter gene driven by the PPAR- $\alpha$  promoter was induced by MG53 overexpression. **G**, Chromatin immunoprecipitation-PCR showed that an enrichment of PPAR- $\alpha$  promoter was detected in the anti-MG53 immunoprecipitated chromatin. Scale bar in **D**, 10  $\mu$ m. Data are mean $\pm$ SEM (\* $P$ <0.05, \*\* $P$ <0.01 vs Ad- $\beta$ -gal; n=3–4 for each group in **A–C** and **F**).

NRVMs, palmitate uptake was repressed (Figure VIIA and VIIB in the online-only Data Supplement). Then, we designed 3 pairs of siRNAs to knockdown PPAR- $\alpha$  expression, and the efficacy of the siRNAs is shown in Figure VIIIA and VIIB in the online-only Data Supplement. PPAR- $\alpha$  silencing abolished MG53-induced uptake of palmitate in NRVMs (Figure 7G and 7H). This result indicates that PPAR- $\alpha$  is an indispensable component for MG53-induced lipid accumulation in MG53 h-TG heart. Altogether, our in vivo and in vitro data have demonstrated that MG53 may

play a crucial role in regulating the expression of PPAR- $\alpha$  and its target genes, thus controlling myocardial lipid metabolism, in addition to its previously reported E3 ligase activity and resultant downregulation of IR and IRS1 and insulin resistance.

### Discussion

The major findings of the present study are that myocardial MG53 expression is elevated in several clinically relevant

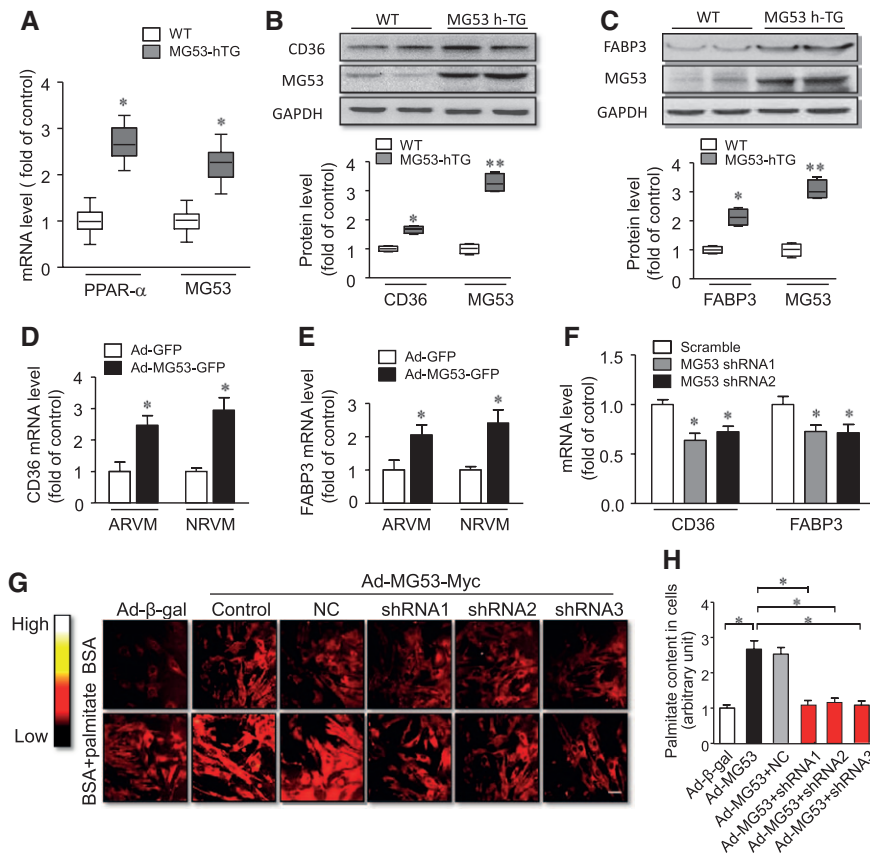


**Figure 7.** MG53 promotes palmitate uptake via enhancing the expression of peroxisome proliferation-activated receptor alpha (PPAR- $\alpha$ ) and its target genes. **A**, mRNA levels of CD36 and FABP3 of wild-type (WT) and hearts from mice with cardiac-specific overexpression of MG53 (MG53 h-TG) were assayed with real-time polymerase chain reaction (PCR). **B** and **C**, In the MG53 h-TG hearts, the CD36 (**B**) and FABP3 (**C**) protein levels were increased as compared with their WT controls. **D** and **E**, In isolated adult and neonatal rat ventricular myocytes (NRVMs), CD36 (**D**) and FABP3 (**E**) mRNA levels were upregulated by adenovirus-mediated MG53 overexpression. **F**, Inhibition of the expression of MG53 with specific shRNAs decreased the mRNA levels of CD36 and FABP3. **G** and **H**, MG53 mediated palmitate uptake was inhibited by PPAR- $\alpha$  gene silencing. Scale bar in **G**, 20  $\mu$ m. NC indicates negative control. Data are mean $\pm$ SEM (\* $P$ <0.05 and \*\* $P$ <0.01 vs WT control for **A–C**, vs Ad-GFP for panels **D** and **E**, vs scramble for **F**, and as indicated in **H**;  $n$ =3–4 for each group in all panels).

animal models with metabolic disorders, and that cardiac-specific overexpression of MG53 is sufficient to produce cardiac phenotypes that closely resemble diabetic cardiomyopathy in mice, including insulin resistance, hypertrophy, ventricular dilation, fibrosis, and cardiac dysfunction. In addition to insulin signaling impairment, MG53 overexpression shifts myocardial energy substrate use further toward lipid dependence. RNA-seq analysis revealed that PPAR- $\alpha$  pathway was activated in the MG53 h-TG hearts, but repressed in the MG53 deficient hearts. We further demonstrated that MG53 regulated PPAR- $\alpha$  expression at a transcriptional level. Thus, the upregulation of PPAR- $\alpha$  and its target genes is responsible for the myocardial lipid accumulation which, in turn, contributes to the diabetic cardiomyopathy-like phenotype.

It is well accepted that in the diabetic heart, the use of glucose is decreased and the oxidation of FFA is increased.<sup>29</sup> The substrate use shift may play an important role in the pathogenesis of diabetic cardiomyopathy. In particular, the increased FFA storage in cardiac myocytes causes lipid toxicity which, in turn, triggers cardiomyocyte death and subsequent fibrosis.<sup>39</sup> In addition, diabetes mellitus-associated elevation of blood glucose may induce glycosylation of certain interstitial

proteins, which may also result in myocardial fibrosis and decreased ventricular compliance.<sup>40,41</sup>

In the present study, we have provided evidence that MG53 is essentially involved in the regulation of cardiac substrate use. Similar to the situation of diabetic heart, the glucose uptake is inhibited, whereas lipid is accumulated and FFA oxidation is enhanced in the cardiomyocytes overexpressing MG53. In line with these findings, genes related to lipid metabolism are upregulated in response to MG53 overexpression. Most importantly, we have provided multiple lines of evidence to demonstrate that MG53 can positively regulate the expression of a key regulator of lipid metabolism, PPAR- $\alpha$ , in the heart and in cultured cardiomyocytes. In fact, the relationship between upregulation of MG53 and the induction of PPAR- $\alpha$  is observed not only in MG53 h-TG hearts but also in hearts from multiple animal models with metabolic disorders, suggesting that MG53-induced cardiac metabolic disorders and resultant diabetic cardiomyopathy is mediated, in part, by upregulation of PPAR- $\alpha$  signaling. This conclusion is supported by the previous notion that PPAR- $\alpha$  overexpression in the heart, indeed, leads to a phenotype that mimics the cardiac symptoms caused by diabetes mellitus in humans, including enhanced FFA uptake and oxidation and suppressed glucose utilization.<sup>34</sup>

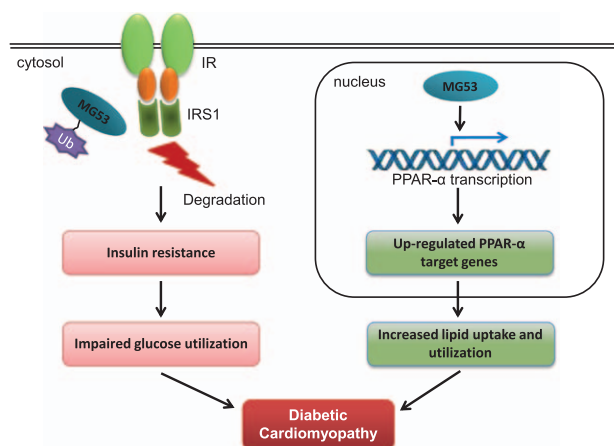


**Figure 8.** Schematic diagram showing signaling pathways involved in MG53-induced diabetic cardiomyopathy. IR indicates insulin receptor; IRS1, insulin receptor substrate 1; PPAR- $\alpha$ , peroxisome proliferation-activated receptor alpha; and Ub, ubiquitin.

We and others have previously shown that MG53 is involved in striated muscle membrane repair,<sup>14,15</sup> and participates in ischemic preconditioning- and postconditioning-mediated cardiac protection.<sup>16,17</sup> Although all the studies, to date, have concentrated on the cytosolic functions of MG53, its role in the nucleus remains elusive. It is noteworthy that several members of the TRIM family play important roles in transcriptional regulation.<sup>42–44</sup> For instance, promyelocytic leukemia can regulate PPAR- $\delta$  expression in hematopoietic stem cells.<sup>45</sup> Some other members travel between the cytosol and nucleus to exert their functions.<sup>46,47</sup>

In this study, we have found that the expression of MG53 is markedly increased in several animal models with metabolic disorders, although the underlying mechanism remains elusive. Candidate mechanisms may include changes in nutrients or genetic defects, or dysregulation of transcription factors or noncoding RNAs under pathological conditions. Thus, the regulation of MG53 expression merits further studies.

In summary, we have demonstrated, for the first time, that overexpression of MG53 induces, whereas its depletion decreases, the mRNA levels of PPAR- $\alpha$  and its target genes. Notably, the PPAR- $\alpha$  promoter is activated by MG53, suggesting that MG53 regulates PPAR- $\alpha$  expression at the transcriptional level. Moreover, inhibition of PPAR- $\alpha$  expression by gene silencing attenuates the MG53-induced lipid uptake in cardiac myocytes, indicating that the dysregulation of lipid metabolism induced by MG53 overexpression is PPAR- $\alpha$  dependent. Taken together, these findings have revealed a previously unappreciated nuclear function of MG53 in regulating the expression of PPAR- $\alpha$  and its target genes. Thus, under pathological conditions, when MG53 expression is increased, it not only compromises myocardial insulin signaling, but also triggers dysregulation of lipid metabolism, both of which contribute to the diabetic cardiomyopathy-like phenotypes (Figure 8).

### Acknowledgments

We express our sincere appreciation to Dr Xiuqin Zhang for the rhesus samples, Dr Jeff Robbins for the cardiac-specific transgenic vector, and Dr Heping Cheng for insightful discussions.

### Sources of Funding

The present study was supported by the National Basic Research Program of China (2013CB531200, 2012CB944500, 2012CB518000), the National Natural Science Foundation of China (81130073, 81170100, 81370234, 81370233, 81370343, 81070674, 81000051, 81270190, and 31221002), and the National Science and Technology Major Projects for “Major New Drugs Innovation and Development” (2013ZX09508104).

### Disclosures

None.

### References

- Wild S, Roglic G, Green A, Sicree R, King H. Global prevalence of diabetes: estimates for the year 2000 and projections for 2030. *Diabetes Care*. 2004;27:1047–1053.
- Rubler S, Dlugash J, Yuceoglu YZ, Kumral T, Branwood AW, Grishman A. New type of cardiomyopathy associated with diabetic glomerulosclerosis. *Am J Cardiol*. 1972;30:595–602.
- Kannel WB, Hjortland M, Castelli WP. Role of diabetes in congestive heart failure: the Framingham study. *Am J Cardiol*. 1974;34:29–34.
- Kannel WB, McGee DL. Diabetes and cardiovascular risk factors: the Framingham study. *Circulation*. 1979;59:8–13.
- Kannel WB, McGee DL. Diabetes and glucose tolerance as risk factors for cardiovascular disease: the Framingham study. *Diabetes Care*. 1979;2:120–126.
- Devereux RB, Roman MJ, Paranicas M, O’Grady MJ, Lee ET, Welty TK, Fabsitz RR, Robbins D, Rhoades ER, Howard BV. Impact of diabetes on cardiac structure and function: the strong heart study. *Circulation*. 2000;101:2271–2276.
- Kannel WB, McGee DL. Diabetes and cardiovascular disease: the Framingham study. *JAMA*. 1979;241:2035–2038.
- Semeniuk LM, Kryski AJ, Severson DL. Echocardiographic assessment of cardiac function in diabetic db/db and transgenic db/db-hGLUT4 mice. *Am J Physiol Heart Circ Physiol*. 2002;283:H976–H982. doi: 10.1152/ajpheart.00088.2002.
- Battiprolu PK, Hojavey B, Jiang N, Wang ZV, Luo X, Iglewski M, Shelton JM, Gerard RD, Rothermel BA, Gillette TG, Lavandero S, Hill JA. Metabolic stress-induced activation of FoxO1 triggers diabetic cardiomyopathy in mice. *J Clin Invest*. 2012;122:1109–1118. doi: 10.1172/JCI60329.
- Carley AN, Semeniuk LM, Shimoni Y, Aasum E, Larsen TS, Berger JP, Severson DL. Treatment of type 2 diabetic db/db mice with a novel PPAR $\gamma$  agonist improves cardiac metabolism but not contractile function. *Am J Physiol Endocrinol Metab*. 2004;286:E449–E455. doi: 10.1152/ajpendo.00329.2003.
- Ouwens DM, Boer C, Fodor M, de Galan P, Heine RJ, Maassen JA, Diamant M. Cardiac dysfunction induced by high-fat diet is associated with altered myocardial insulin signalling in rats. *Diabetologia*. 2005;48:1229–1237. doi: 10.1007/s00125-005-1755-x.
- Song R, Peng W, Zhang Y, Lv F, Wu HK, Guo J, Cao Y, Pi Y, Zhang X, Jin L, Zhang M, Jiang P, Liu F, Meng S, Zhang X, Jiang P, Cao CM, Xiao RP. Central role of E3 ubiquitin ligase MG53 in insulin resistance and metabolic disorders. *Nature*. 2013;494:375–379. doi: 10.1038/nature11834.
- Yi JS, Park JS, Ham YM, Nguyen N, Lee NR, Hong J, Kim BW, Lee H, Lee CS, Jeong BC, Song HK, Cho H, Kim YK, Lee JS, Park KS, Shin H, Choi I, Lee SH, Park WJ, Park SY, Choi CS, Lin P, Karunasiri M, Tan T, Duann P, Zhu H, Ma J, Ko YG. MG53-induced IRS-1 ubiquitination negatively regulates skeletal myogenesis and insulin signalling. *Nat Commun*. 2013;4:2354. doi: 10.1038/ncomms3354.
- Cai C, Masumiya H, Weisleder N, Matsuda N, Nishi M, Hwang M, Ko JK, Lin P, Thornton A, Zhao X, Pan Z, Komazaki S, Brotto M, Takeshima H, Ma J. MG53 nucleates assembly of cell membrane repair machinery. *Nat Cell Biol*. 2009;11:56–64. doi: 10.1038/ncb1812.
- Wang X, Xie W, Zhang Y, Lin P, Han L, Han P, Wang Y, Chen Z, Ji G, Zheng M, Weisleder N, Xiao RP, Takeshima H, Ma J, Cheng H. Cardioprotection of ischemia/reperfusion injury by cholesterol-dependent MG53-mediated membrane repair. *Circ Res*. 2010;107:76–83. doi: 10.1161/CIRCRESAHA.109.215822.
- Cao CM, Zhang Y, Weisleder N, Ferrante C, Wang X, Lv F, Zhang Y, Song R, Hwang M, Jin L, Guo J, Peng W, Li G, Nishi M, Takeshima H, Ma J, Xiao RP. MG53 constitutes a primary determinant of cardiac ischemic preconditioning. *Circulation*. 2010;121:2565–2574. doi: 10.1161/CIRCULATIONAHA.110.954628.

17. Zhang Y, Lv F, Jin L, Peng W, Song R, Ma J, Cao CM, Xiao RP. MG53 participates in ischaemic postconditioning through the RISK signalling pathway. *Cardiovasc Res*. 2011;91:108–115. doi: 10.1093/cvr/cvr029.
18. Freudiger CW, Min W, Saar BG, Lu S, Holtom GR, He C, Tsai JC, Kang JX, Xie XS. Label-free biomedical imaging with high sensitivity by stimulated Raman scattering microscopy. *Science*. 2008;322:1857–1861. doi: 10.1126/science.1165758.
19. Yu Z, Chen T, Zhang X, Fu D, Liao X, Shen J, Liu X, Zhang B, Xie XS, Su X-D, Chen J, Huang Y. Label-free chemical imaging in vivo: three-dimensional non-invasive microscopic observation of amphioxus notochord through stimulated Raman scattering (SRS). *Chemical Science*. 2012;3:2646–2654.
20. Moyers JS, Bilan PJ, Reynet C, Kahn CR. Overexpression of Rad inhibits glucose uptake in cultured muscle and fat cells. *J Biol Chem*. 1996;271:23111–23116.
21. Zhang SJ, Liu CJ, Yu P, Zhong X, Chen JY, Yang X, Peng J, Yan S, Wang C, Zhu X, Xiong J, Zhang YE, Tan BC, Li CY. Evolutionary interrogation of human biology in well-annotated genomic framework of rhesus macaque. *Mol Biol Evol*. 2014;31:1309–1324. doi: 10.1093/molbev/msu084.
22. Huang da W, Sherman BT, Lempicki RA. Systematic and integrative analysis of large gene lists using DAVID bioinformatics resources. *Nat Protoc*. 2009;4:44–57. doi: 10.1038/nprot.2008.211.
23. Huang da W, Sherman BT, Lempicki RA. Bioinformatics enrichment tools: paths toward the comprehensive functional analysis of large gene lists. *Nucleic Acids Res*. 2009;37:1–13.
24. Lee CS, Yi JS, Jung SY, Kim BW, Lee NR, Choo HJ, Jang SY, Han J, Chi SG, Park M, Lee JH, Ko YG. TRIM72 negatively regulates myogenesis via targeting insulin receptor substrate-1. *Cell Death Differ*. 2010;17:1254–1265. doi: 10.1038/cdd.2010.1.
25. Cross DA, Alessi DR, Cohen P, Andjelkovich M, Hemmings BA. Inhibition of glycogen synthase kinase-3 by insulin mediated by protein kinase B. *Nature*. 1995;378:785–789. doi: 10.1038/378785a0.
26. Kohn AD, Kovacina KS, Roth RA. Insulin stimulates the kinase activity of RAC-PK, a pleckstrin homology domain containing ser/thr kinase. *EMBO J*. 1995;14:4288–4295.
27. Gertz EW, Wisneski JA, Stanley WC, Neese RA. Myocardial substrate utilization during exercise in humans: dual carbon-labeled carbohydrate isotope experiments. *J Clin Invest*. 1988;82:2017–2025. doi: 10.1172/JCI113822.
28. Saddik M, Lopaschuk GD. Myocardial triglyceride turnover and contribution to energy substrate utilization in isolated working rat hearts. *J Biol Chem*. 1991;266:8162–8170.
29. Razeghi P, Young ME, Cockrill TC, Frazier OH, Taegtmeier H. Downregulation of myocardial myocyte enhancer factor 2C and myocyte enhancer factor 2C-regulated gene expression in diabetic patients with nonischemic heart failure. *Circulation*. 2002;106:407–411.
30. Young ME, Guthrie PH, Razeghi P, Leighton B, Abbasi S, Patil S, Youker KA, Taegtmeier H. Impaired long-chain fatty acid oxidation and contractile dysfunction in the obese Zucker rat heart. *Diabetes*. 2002;51:2587–2595.
31. Buchanan J, Mazumder PK, Hu P, Chakrabarti G, Roberts MW, Yun UJ, Cooksey RC, Litwin SE, Abel ED. Reduced cardiac efficiency and altered substrate metabolism precedes the onset of hyperglycemia and contractile dysfunction in two mouse models of insulin resistance and obesity. *Endocrinology*. 2005;146:5341–5349. doi: 10.1210/en.2005-0938.
32. How OJ, Aasum E, Severson DL, Chan WY, Essop MF, Larsen TS. Increased myocardial oxygen consumption reduces cardiac efficiency in diabetic mice. *Diabetes*. 2006;55:466–473.
33. Djouadi F, Weinheimer CJ, Saffitz JE, Pitchford C, Bastin J, Gonzalez FJ, Kelly DP. A gender-related defect in lipid metabolism and glucose homeostasis in peroxisome proliferator-activated receptor alpha-deficient mice. *J Clin Invest*. 1998;102:1083–1091. doi: 10.1172/JCI3949.
34. Finck BN, Lehman JJ, Leone TC, Welch MJ, Bennett MJ, Kovacs A, Han X, Gross RW, Kozak R, Lopaschuk GD, Kelly DP. The cardiac phenotype induced by PPARalpha overexpression mimics that caused by diabetes mellitus. *J Clin Invest*. 2002;109:121–130. doi: 10.1172/JCI14080.
35. Zhang X, Zhang R, Raab S, Zheng W, Wang J, Liu N, Zhu T, Xue L, Song Z, Mao J, Li K, Zhang H, Zhang Y, Han C, Ding Y, Wang H, Hou N, Liu Y, Shang S, Li C, Sebokova E, Cheng H, Huang PL. Rhesus macaques develop metabolic syndrome with reversible vascular dysfunction responsive to pioglitazone. *Circulation*. 2011;124:77–86. doi: 10.1161/CIRCULATIONAHA.110.990333.
36. Shi Y, Downes M, Xie W, Kao HY, Ordentlich P, Tsai CC, Hon M, Evans RM. Sharp, an inducible cofactor that integrates nuclear receptor repression and activation. *Genes Dev*. 2001;15:1140–1151. doi: 10.1101/gad.871201.
37. Sorrentino D, Robinson RB, Kiang CL, Berk PD. At physiologic albumin/oleate concentrations oleate uptake by isolated hepatocytes, cardiac myocytes, and adipocytes is a saturable function of the unbound oleate concentration: uptake kinetics are consistent with the conventional theory. *J Clin Invest*. 1989;84:1325–1333. doi: 10.1172/JCI114301.
38. Coburn CT, Knapp FF Jr, Febbraio M, Beets AL, Silverstein RL, Abumrad NA. Defective uptake and utilization of long chain fatty acids in muscle and adipose tissues of CD36 knockout mice. *J Biol Chem*. 2000;275:32523–32529. doi: 10.1074/jbc.M003826200.
39. Bugger H, Abel ED. Molecular mechanisms of diabetic cardiomyopathy. *Diabetologia*. 2014;57:660–671. doi: 10.1007/s00125-014-3171-6.
40. Nunoda S, Genda A, Sugihara N, Nakayama A, Mizuno S, Takeda R. Quantitative approach to the histopathology of the biopsied right ventricular myocardium in patients with diabetes mellitus. *Heart Vessels*. 1985;1:43–47.
41. Syrový I, Hodný Z. Non-enzymatic glycosylation of myosin: effects of diabetes and ageing. *Gen Physiol Biophys*. 1992;11:301–307.
42. Tsai WW, Wang Z, Yiu TT, Akdemir KC, Xia W, Winter S, Tsai CY, Shi X, Schwarzer D, Plunkett W, Aronow B, Gozani O, Fischle W, Hung MC, Patel DJ, Barton MC. TRIM24 links a non-canonical histone signature to breast cancer. *Nature*. 2010;468:927–932. doi: 10.1038/nature09542.
43. Zoumpoulidou G, Broceño C, Li H, Bird D, Thomas G, Mittnacht S. Role of the tripartite motif protein 27 in cancer development. *J Natl Cancer Inst*. 2012;104:941–952. doi: 10.1093/jnci/djs224.
44. Abrink M, Ortiz JA, Mark C, Sanchez C, Looman C, Hellman L, Chambon P, Losson R. Conserved interaction between distinct Krüppel-associated box domains and the transcriptional intermediary factor 1 beta. *Proc Natl Acad Sci USA*. 2001;98:1422–1426. doi: 10.1073/pnas.041616998.
45. Ito K, Carracedo A, Weiss D, Arai F, Ala U, Avigan DE, Schafer ZT, Evans RM, Suda T, Lee CH, Pandolfi PP. A PML–PPAR- $\delta$  pathway for fatty acid oxidation regulates hematopoietic stem cell maintenance. *Nat Med*. 2012;18:1350–1358. doi: 10.1038/nm.2882.
46. Bell JL, Malyukova A, Kavallaris M, Marshall GM, Cheung BB. TRIM16 inhibits neuroblastoma cell proliferation through cell cycle regulation and dynamic nuclear localization. *Cell Cycle*. 2013;12:889–898. doi: 10.4161/cc.23825.
47. Yuan Z, Villagra A, Peng L, Coppola D, Glozak M, Sotomayor EM, Chen J, Lane WS, Seto E. The ATDC (TRIM29) protein binds p53 and antagonizes p53-mediated functions. *Mol Cell Biol*. 2010;30:3004–3015. doi: 10.1128/MCB.01023-09.

### CLINICAL PERSPECTIVE

Diabetic cardiomyopathy has become a major cause of heart failure. In the present study, we have demonstrated that increased MG53 protein level in the transgenic mouse heart results in diabetic cardiomyopathy–like phenotypes. Mechanistically, MG53 not only acts as an E3 ligase to target insulin receptor and insulin receptor substrate 1, resulting in insulin signaling deterioration, but also constitutes a positive regulator of peroxisome proliferation-activated receptor alpha and its target genes, leading to myocardial substrate utilization shift to free fatty acids and ultimately cardiac remodeling and dysfunction. Indeed, the upregulation of MG53 in the heart is consistently accompanied by an elevation of peroxisome proliferation-activated receptor alpha abundance in all of the tested metabolic disease models from mouse to nonhuman primates. These findings not only reveal a novel function of MG53, but also mark the MG53–peroxisome proliferation-activated receptor alpha signaling pathway as a potentially important therapeutic target for the treatment of diabetes mellitus and associated diabetic cardiomyopathy. It awaits future studies to determine whether therapies that will correct abnormal myocardial substrate use in diabetes mellitus will translate to lower prevalence of heart failure or improved long-term survival.

## **SUPPLEMENTAL MATERIAL**

## **Supplemental Material and Methods**

### **Animals**

The generation of MG53-null mice was described previously<sup>1</sup>. Adult Sprague-Dawley rats and neonatal rats were from Vital River Laboratory Animal Technology Co. Ltd. All the animals had free access to water and standard rodent chow (11.4% calories from fat, Academy of Military Medical Sciences, China).

### **Cardiomyocyte isolation**

The ventricles of the neonatal rat heart were collected, and the cardiomyocytes were isolated by enzymatic digestion as described before<sup>2</sup>. Adult male Sprague-Dawley rats were anesthetized with 4% chloral hydrate (1ml/100g body weight), and cardiomyocytes were isolated by enzymatic digestion by retrograde perfusion through the aorta as reported previously<sup>3</sup>. Freshly-isolated cardiomyocytes were plated in culture dishes coated with laminin (Sigma) for 1hr and then the attached cells were maintained in M199 medium (Sigma) supplemented with 5mM creatine, 2mM L-carnitine, 5mM taurine, 25mM Hepes (all from Sigma).

### **Western blots analysis**

Antibodies against MG53 (Abcam and Abnova), PPAR- $\alpha$  (Abcam), CD36 (Abcam), FABP3 (Boster) were used to detect the corresponding proteins. Horseradish peroxidase (HRP)-conjugated secondary antibodies (rabbit anti-mouse or goat anti-rabbit) were used. The abundance of the proteins was determined by measuring the signal intensity using Image J software (NIH, Bethesda, MD).

### **Subcellular fractionation**

A nuclear/cytosol fractionation kit (Biovision) was used to prepare nuclear and cytosolic extracts of cells or tissue samples. NRVMs ( $2 \times 10^6$ ) were rinsed twice with cold PBS before scraped from the culture plate. About 10mg of heart tissue was homogenized with a Polytron ultrasonic homogenizer to prepare nuclear and cytosolic lysates. All the subsequent procedures were performed according to the protocols provided by the manufacturer.

### **Transfection for dual-luciferase reporter assay**

Different PPAR- $\alpha$  reporter constructs were transfected into H9c2 cells using Lipofectamine 3000 (Invitrogen). The cells were infected with adenovirus expressing either  $\beta$ -gal or MG53-Myc immediately after transfection. Forty-eight hours after transfection, the cells were lysed with positive lysis buffer (Promega). The firefly and Renilla luciferase activities in the lysate were determined using a luminometer. The readings of the firefly luciferase activity were normalized to that of Renilla to determine the activity of the PPAR- $\alpha$  reporter constructs.

### **Western blot analysis**

Whole-cell lysates or tissue lysates were extracted in RIPA buffer (in mM, 20 Tris-HCl, pH 7.5; 150 NaCl; 1 EDTA; 1 EGTA; 2.5 sodium pyrophosphate; 1  $\beta$ -glycerophosphate; 1  $\text{Na}_3\text{VO}_4$ ; 1% Triton X-100; and 0.5% sodium deoxycholate supplemented with 1mM PMSF and 1mM protease inhibitor cocktail before use). All the lysates were resolved on 10% SDS-PAGE gels and then transferred to PVDF membrane (Bio-Rad). Specific first and second antibodies were used to detect the protein of interest.

### **Histological analysis and confocal immuno-fluorescence imaging**

The hearts were fixed in 4% paraformaldehyde (pH 7.4) overnight for histological analysis, embedded in paraffin, and serially sectioned at 5 $\mu$ m. Standard hematoxylin and eosin staining was used. After NRVMs were plated on glass slides at an appropriate density, they were fixed with 4% paraformaldehyde (pH 7.4) for 10min, permeabilized with 0.1% Triton dissolved in PBS for 10min at room temperature, and incubated overnight in blocking solution containing antibody against MG53. A second antibody labeled with fluorescein isothiocyanate was applied to detect the endogenous MG53 protein. All the immune-fluorescence images were captured by a laser scanning confocal microscope system (LSM-700, Zeiss).

### **Plasmids and transfection**

Adenovirus expressing GFP or MG53-GFP was described previously<sup>1</sup>. The PPAR- $\alpha$  promoter was amplified from rat genomic DNA, and sub-cloned into pGL3-Basic vector (Promega) between the KpnI (NEB) and NheI (NEB) sites. The full-length mouse MG53 and GFP cDNA was inserted into pM vector (CloneTech) between the Sall and XbaI sites.

### **SRS microscopy for palmitate uptake measurement**

The lipid uptake by cardiomyocytes was assayed using a stimulated Raman scattering (SRS) system. In the SRS microscope system, a pump laser integrated Optical Parametric Oscillator (OPO), also known as one-box OPO (APE, Berlin, Germany) serves as light source. It provides synchronized and spatially overlapped pump and Stokes pulse trains at repetition rate of 76 MHz. The pump beam is continuously tunable from 780 nm to 990 nm; however the Stokes beam is fixed at 1064 nm. The

Stokes beam is modulated by an electro-optic modulator (EO-AM-R-20-C2, Thorlabs, USA) at frequency of 20.2 MHz. The collinearly overlapped beams are directed into an inverted multi-photon microscope (IX81/FV1000, Olympus, Japan). Lasers are focused on the sample by a 60X water immersion objective (UPLSAPO 60XW, Olympus, Japan) and scanned to acquire image. The transmission light is collected by a water immersion condenser (N.A. 0.9, Olympus, Japan), and then filtered by a band-pass filter (890/220m, Chroma, USA) to remove Stokes beam. The pump beam is detected by a large area photodiode (FDS1010, Thorlabs, USA) reverse-biased at 75 V. The voltage signal generated by photodiode is sent into a lock-in amplifier (HF2LI, Zurich Instrument, Switzerland). Demodulated signal is fed back into the microscope software (FV10-ASW, Olympus, Japan) for image reconstruction. Cells were cultured in 35 mm Petri dishes with glass bottom, and scanned with the SRS system described above. To probe the palmitate content, pump and probe frequency difference was tuned to  $2850\text{ cm}^{-1}$ , which was in resonance with the  $\text{CH}_2$  symmetric vibration mode in live cells. For each Petri dish, 3-4 random fields were selected for imaging. Three-dimensional images were acquired in each field,  $\sim 3$  min per stack, to obtain complete information of palmitate distribution. During image acquisition, cells were kept at  $37^\circ\text{C}$  within a live cell incubator (Chamlide, LCI, Korea)<sup>4</sup>.

## **ChIP**

$2 \times 10^6$  cells were cross-linked in 1% formaldehyde for each ChIP. After washing with cold PBS, cells were homogenized with a sonicator on ice in cell lysis buffer supplemented with 0.2% NP-40 and protease inhibitors (1mM PMSF and 1mM cocktail). DNA was sheared into fragments ranging between 200 and 800bp. After centrifugation, the supernatant was diluted by 10-fold with dilution buffer, and 1% of the diluted solution was reserved for control. The remaining lysate was pre-cleaned by adding 75 $\mu\text{l}$  salmon sperm DNA/protein A agarose and agitated for 30 min at  $4^\circ\text{C}$ . A control IgG or the primary antibody against MG53 was added to the pre-cleaned

supernatant. The supernatant was incubated overnight at 4 °C with constant rotation. Immunoprecipitated complex was collected after addition of 60µl salmon sperm DNA/protein A agarose. The complex was washed 6 times, treated with proteinase K for 1 hour, and reverse cross-linked by heating at 65° C for 4 hours. The immunoprecipitated DNA was purified by phenol/chloroform extraction and recovered for PCR reaction<sup>5,6</sup>.

**Supplementary Table 1.****Primers for qPCR**

<b>Genes</b>	<b>Sense primers (5'-3')</b>	<b>Antisense primers (5'-3')</b>
18S rRNA	GGAAGGGCACCACCAGGAGT	TGCAGCCCCGGACATCTAAG
Mouse ANP	GCTTCCAGGCCATATTGGAGCA	TCTCTCAGAGGTGGGTTGACCT
Mouse BNP	ATGGATCTCCTGAAGGTGCTGT	GCAGCTTGAGATATGTGTCACC
Mouse $\alpha$ -MHC	GGATCCACTTTGGAGCTACT	TCAGCATCTTCTGTGCCATC
Mouse $\beta$ -MHC	TACATGCTGACAGATCGGGA	CATGTCTAGAAGCTCAGGCT
Mouse Glut4	TACGGTCTTCACGTTGGTCT	CACGATGGAGACATAGCTCA
Mouse PDK 1	AATGCCATGAGAGCGACCAT	GTGCGGTTGAGTACATGTAG
Mouse PDK 2	AGAGATCAACCTGCTTCCTG	CCATAGGTGTCCTTGACTC
Mouse PDK 3	TGGTAGCTCCAGAGCTAGAA	ACTCCACCACCTAGGTCACT
Mouse Pdha1	CGAGAGGCAACAAAGTTTGC	TTGCAAGATTGCTGTTCCACC
Mouse PDC-E2	GGTAGCTCCTATCCTACTCA	AACATCCCTTGTGCCTTCAG
Mouse Crat	GAACGCCTACAGAAGGGACT	CACCCTCGATGAGTTTGGCA
Mouse Acadvl	ATCAGGTGTTCCCATACCCA	TCCTTGAGTCCCTGCAAAGT
Mouse Acaa2	TCAACAGGCTCTGTGGCTCT	TGCCACAAAGTATCTTCC
Mouse Ppargc1a	ATCTCTTCTCTGACCCCAG	TCTTGCAAGAGGGCTTCAGC
Mouse Acs11	AACGAGGCAAGAAGTGTGGG	TGGTGAGTGATCATTGCTCC
Mouse Acadm	AGGATGACGGAGCAGCCAAT	ATCTGGGTAGAACGTGCCA
Mouse Acacb	ATCGACATGTACGGCCACCA	CTGCAGGCTGTTTAGCTCGT

Mouse Cpt-1b	CGTTCACGCCATGATCATGT	AGAGCCAGACCTTGAAGAAG
Rat CD36	GTCCTTGAAGAAGGAACCATTGC	CACAGCCAGATTGAGAACTGTGA
Rat PPAR- $\alpha$	TCCCCACTTGAAGCAGATGA	CTCGATGTTTCAGTGCATTGC
Rat FABP3	CTTTGTCGGTACCTGGAAG	ACTTCTGCACATGGACCAG

**Supplementary Table 2.**

**Sequences of the siRNAs against PPAR- $\alpha$**

siRNA1	Sense (5'-3')	CGAUCUGAAAGAUUCGGAAACUGCA
	Antisense (5'-3')	UGCAGUUUCCGAAUCUUUCAGAUCG
siRNA2	Sense (5'-3')	GAGCUCACGGAAUUUGCCAAGGCUA
	Antisense (5'-3')	UAGCCUUGGCAAUUCCGUGAGCUC
siRNA3	Sense (5'-3')	CCAGGCUUUGCAAACUUGGACUUGA
	Antisense (5'-3')	UCAAGUCCAAGUUUGCAAAGCCUGG

### Supplementary Table 3.

#### Primers for PPAR- $\alpha$ promoter

Primers1	forward	+43 ACACGCTAGGAAGGGCACACGCGT
	reverse	+119 ACCCAGCGTCGCTTCAGTTCCA
Primers2	forward	-140 ACAGTGAGGTGGGTGGACAGGGA
	reverse	-2 GACTCGAAGTAGCGGACAGTTCCA
Primers3	forward	-248 TACCCGGGCGGGCTGGCCCTG
	reverse	-85 AAAGTCGCACGCGTGTGCCCTT
Primers4	forward	-353 GGCACGGGCGCGCGTAGGCGGT
	reverse	-160 CTCCCGTCCTCGCGCGTGCCCT
Primers5	forward	-473 GTGTGTCTCGTTCTGAACCGC
	reverse	-289 AGCGGCTGTCTCCGCCCCCGT

**Supplementary Table 4.****Ventricular function of MG53 h-TG mice**

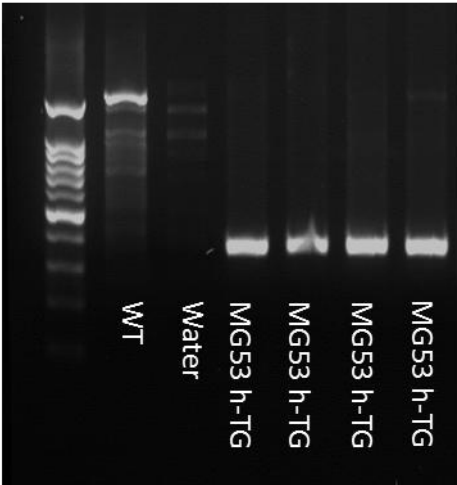
	WT	MG53 h-TG
HR (bpm)	417.2±14.1	390.4±13.2
EF (%)	62.67±1.15	45.86±1.93**
FS (%)	33.40±0.84	22.66±±1.13**
IVSd	0.86±0.01	0.92±0.01*
IVSs	1.36±0.02	1.26±0.02*
LVIDd	3.88±0.07	4.09±0.13
LVIDs	2.59±0.07	3.17±0.12**
LVPWd	0.86±0.02	0.87±0.02
LVPWs	1.31±0.02	1.18±0.03**

Data are presented as mean ± s.e.m. \**p* <0.05, \*\**p* <0.01 vs WT control, and n = 10-12.

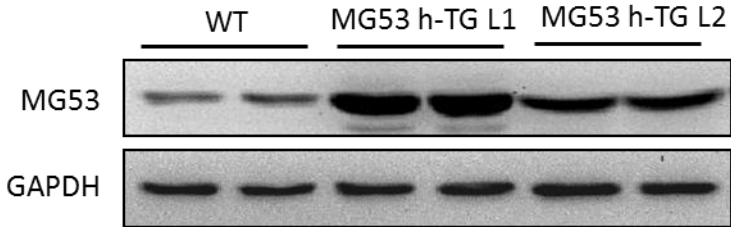
HR, heart rate; EF, ejection fraction; FS, fractional shortening; IVSd interventricular septum at diastole; IVSs, interventricular septum at systole; LVIDd, LV internal diameter at diastole; LVIDs, LV internal diameter at systole; LVPWd, LV posterior wall thickness at diastole; LVPWs, LV posterior wall thickness at systole.

# Supplementary Figure 1

**A**

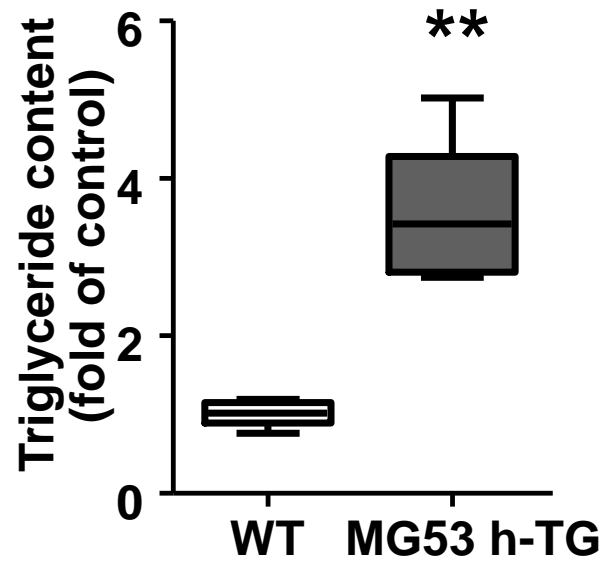


**B**

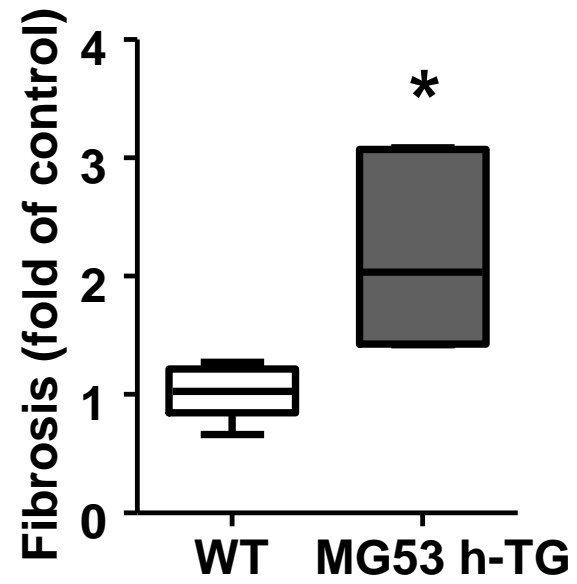


## Supplementary Figure 2

**A**

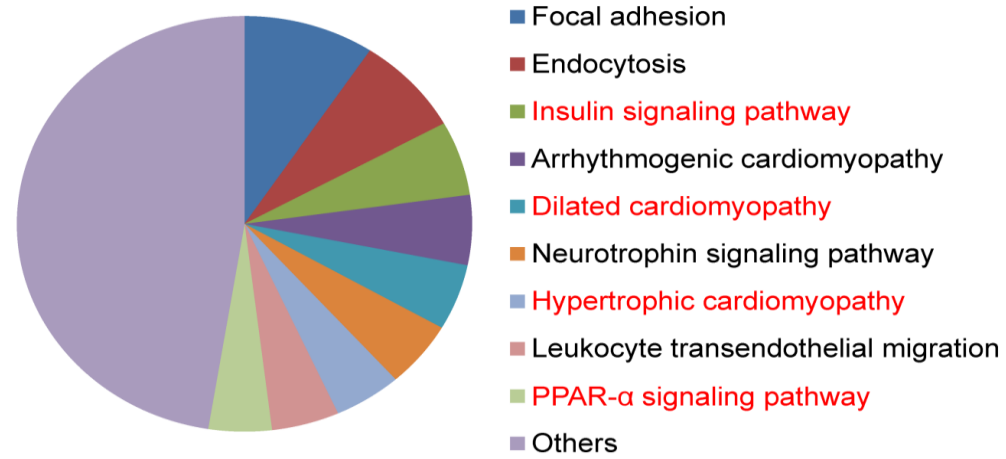


**B**

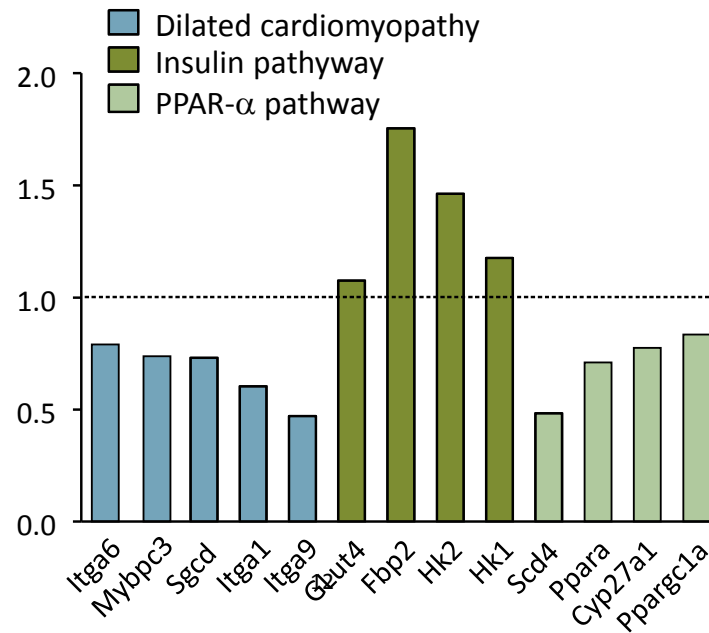


# Supplementary Figure 3

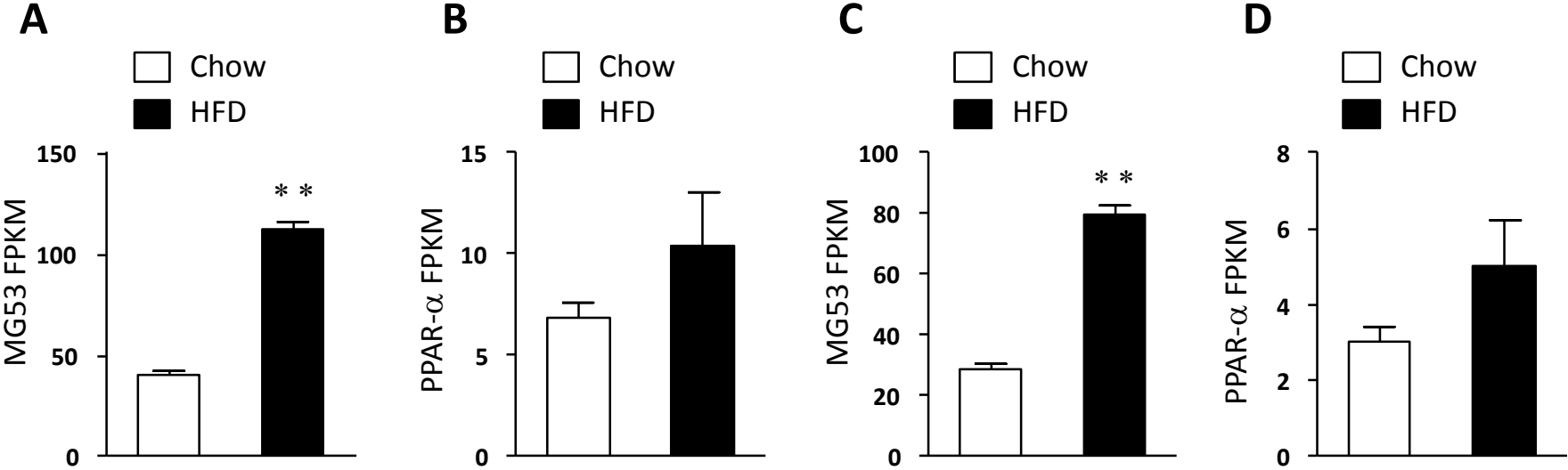
**A**



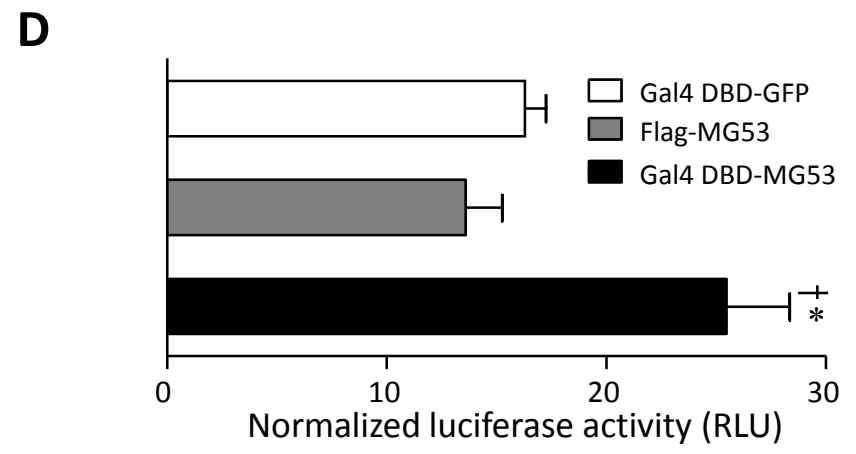
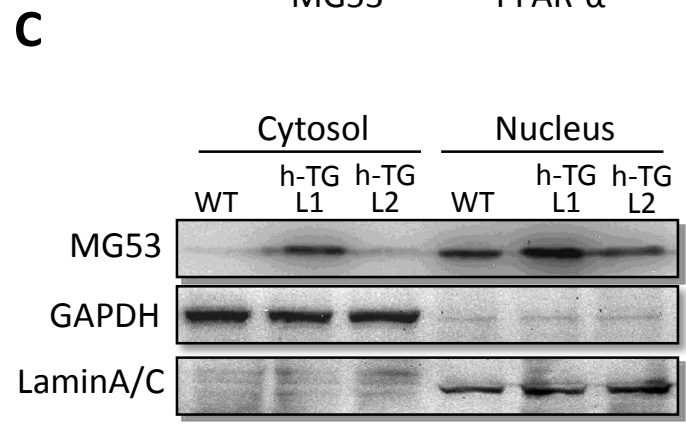
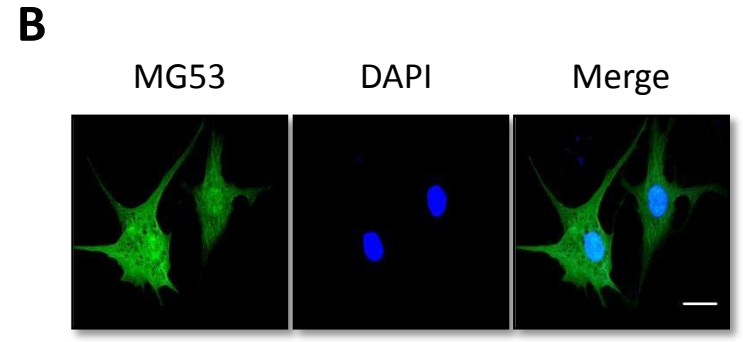
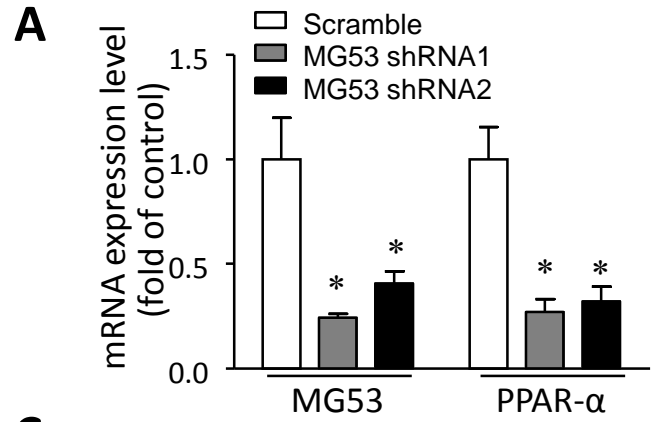
**B**



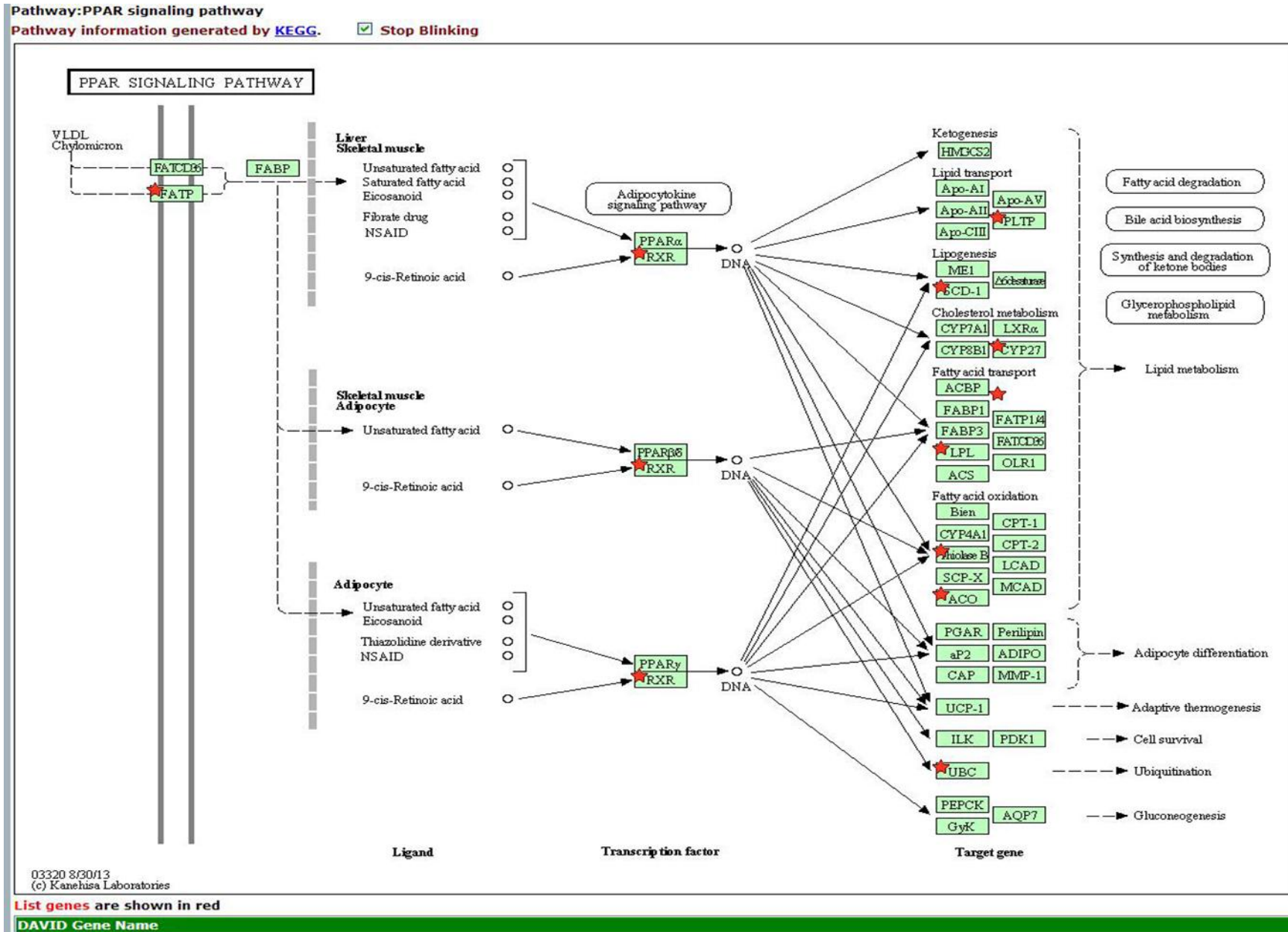
# Supplementary Figure 4



# Supplementary Figure 5

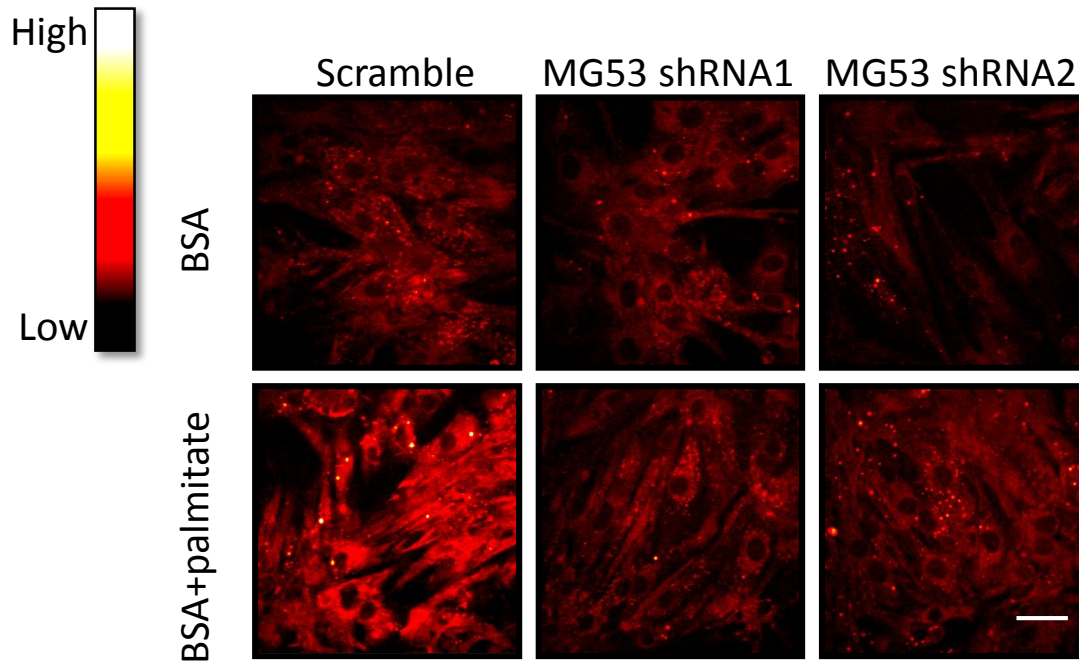


# Supplementary Figure 6

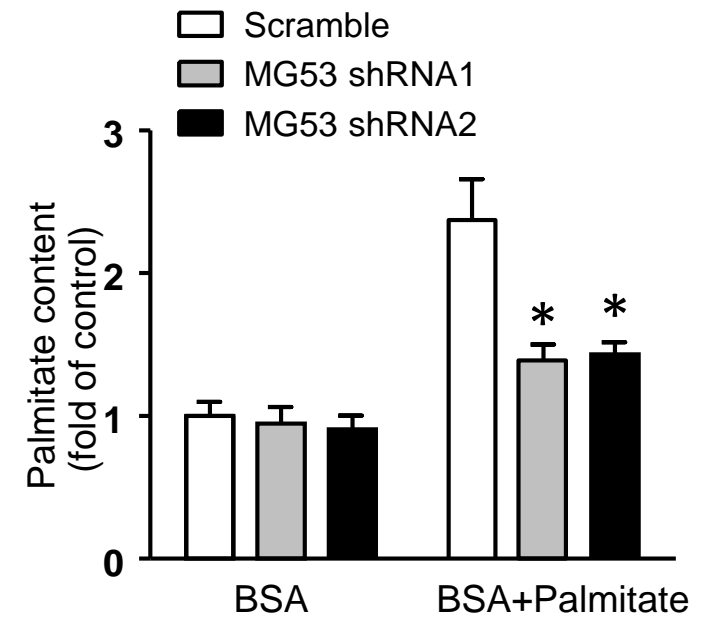


# Supplementary Figure 7

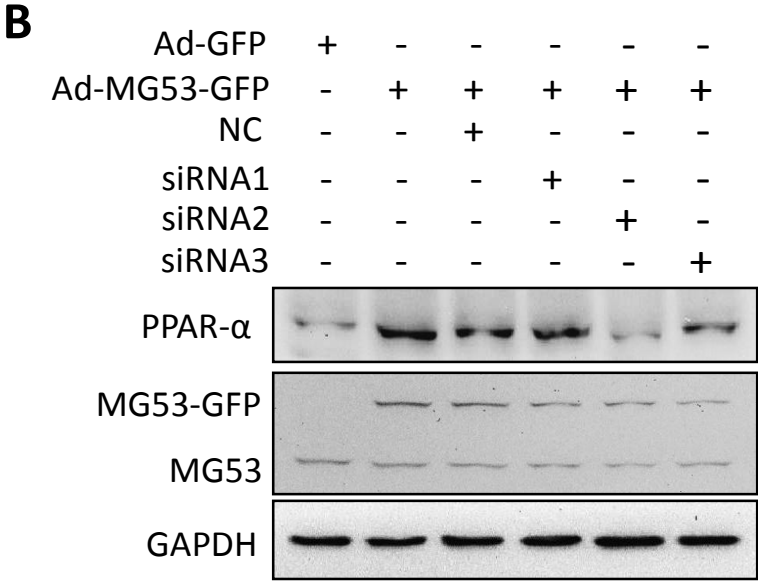
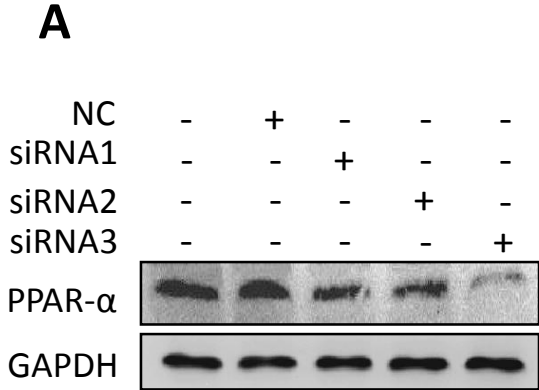
**A**



**B**



# Supplementary Figure 8



## Supplementary Figure Legend

**Supplementary Figure 1. Genotyping and myocardial MG53 protein levels in MG53 h-TG mice.** (A) Genotyping was performed by PCR using the specific primers, upstream (5'-ctcgagctgctgtttgctttc-3') and downstream (5'- ccgctctagaactagtgatc-3'). MG53 h-TG transgenic mice had a specific band at ~400 bp. (B) Myocardial MG53 protein levels of the two MG53 h-TG lines.

**Supplementary Figure 2. Quantitation results of neutral triglyceride deposition and fibrosis in MG53 h-TG hearts.** (A) Increase of triglyceride content in MG53 h-TG hearts as compared with WT. (B) Increase of fibrosis in MG53 h-TG hearts. \*,  $p < 0.05$ ; \*\*,  $p < 0.01$  vs. WT littermates. n=6-8

**Supplementary Figure 3. RNA-Seq analysis of MG53 KO mice and their WT controls** (A) Categories of genes influenced by MG53 deficiency according to DAVID analysis. (B) Changes of the genes belonging to dilated cardiomyopathy, the insulin signaling pathway, and the PPAR- $\alpha$  pathway.

**Supplementary Figure 4. RNA-Seq data showed an up-regulation of MG53 and PPAR- $\alpha$  in 35-week-old mice on an HFD.** (A, B) Relative mRNA levels of samples from hearts. (C, D) Relative mRNA levels of samples from skeletal muscle.

**Supplementary Figure 5. MG53 regulates PPAR- $\alpha$  expression at the transcriptional level.** (A) Real-time PCR showed that the PPAR- $\alpha$  mRNA level was down-regulated when MG53 was knocked down with two effective shRNAs. (B) In NRVMs, the MG53-GFP fusion protein displayed a universal distribution. (C) Western blots of the

cytosolic and nuclear fractions of hearts from WT or MG53 h-TG mice. (D) The Gal4 DBD-MG53 fusion protein activated a Gal4-responsive reporter when co-transfected into H9c2 cells. Data in A and C are mean  $\pm$  s.e.m. \* $p$  <0.05 vs scrambled shRNA,  $^{\dagger}$   $p$  <0.05 vs Flag-MG53 and  $n = 6-8$ . Scale bar in B, 20  $\mu$ m.

**Supplementary Figure 6. Changes of genes belonging to PPAR family revealed by DAVID analysis.** 916 genes with RPKM >0.5 and  $p$  <0.05 were selected, and uploaded for online DAVID analysis (<http://david.abcc.ncifcrf.gov/>). After mapping the DAVID analysis results back to the KEGG database, the PPAR signaling pathway was shown to be significantly altered in the MG53 h-TG heart as compared with WT controls. Green boxes indicate genes involved in the pathways. Red stars indicate genes whose expression was significantly changed.

**Supplementary Figure 7. MG53 deficiency led to decreased palmitate uptake by NRVMs.** Gene silencing of MG53 by specific shRNA significantly decreased palmitate uptake. \*,  $p$  <0.05 vs. scrambled shRNA.  $n=6-7$

**Supplementary Figure 8. The efficacy of siRNA against PPAR- $\alpha$ .** (A) Western blot showed that the PPAR- $\alpha$  protein level was significantly decreased by the three specific siRNAs. (B) The increase in the PPAR- $\alpha$  protein level induced by MG53 overexpression was attenuated by siRNAs against PPAR- $\alpha$ . NC, non-specific siRNA control.

## References:

1. Cai C, Masumiya H, Weisleder N, Matsuda N, Nishi M, Hwang M, Ko JK, Lin P, Thornton A, Zhao X, Pan Z, Komazaki S, Brotto M, Takeshima H, Ma J. MG53 nucleates assembly of cell membrane repair machinery. *Nat Cell Biol.* 2009;11:56-64
2. Cross DA, Alessi DR, Cohen P, Andjelkovich M, Hemmings BA. Inhibition of glycogen synthase kinase-3 by insulin mediated by protein kinase B. *Nature.* 1995;378:785-789
3. Pasumarthi KB, Field LJ. Cardiomyocyte cell cycle regulation. *Circ Res.* 2002;90:1044-1054
4. Fu D, Lu FK, Zhang X, Freudiger C, Pernik DR, Holtom G, Xie XS. Quantitative chemical imaging with multiplex stimulated Raman scattering microscopy. *J Am Chem Soc.* 2012;134:3623-3626
5. Lynch MD, Smith AJ, De Gobbi M, Flenley M, Hughes JR, Vernimmen D, Ayyub H, Sharpe JA, Sloane-Stanley JA, Sutherland L, Meek S, Burdon T, Gibbons RJ, Garrick D, Higgs DR. An interspecies analysis reveals a key role for unmethylated CpG dinucleotides in vertebrate polycomb complex recruitment. *EMBO J.* 2012;31:317-329
6. Singh NP, Madabhushi SR, Srivastava S, Senthilkumar R, Neeraja C, Khosla S, Mishra RK. Epigenetic profile of the euchromatic region of human Y chromosome. *Nucleic Acids Res.* 2011;39:3594-3606

## Upregulation of MG53 Induces Diabetic Cardiomyopathy Through Transcriptional Activation of Peroxisome Proliferation-Activated Receptor $\alpha$

Fenghua Liu, Ruisheng Song, Yuanqing Feng, Jiaojiao Guo, Yanmin Chen, Yong Zhang, Tao Chen, Yanru Wang, Yanyi Huang, Chuan-Yun Li, Chunmei Cao, Yan Zhang, Xinli Hu and Rui-ping Xiao

*Circulation*. 2015;131:795-804; originally published online January 30, 2015;  
doi: 10.1161/CIRCULATIONAHA.114.012285

*Circulation* is published by the American Heart Association, 7272 Greenville Avenue, Dallas, TX 75231  
Copyright © 2015 American Heart Association, Inc. All rights reserved.  
Print ISSN: 0009-7322. Online ISSN: 1524-4539

The online version of this article, along with updated information and services, is located on the World Wide Web at:

<http://circ.ahajournals.org/content/131/9/795>

Data Supplement (unedited) at:

<http://circ.ahajournals.org/content/suppl/2015/01/30/CIRCULATIONAHA.114.012285.DC1.html>

**Permissions:** Requests for permissions to reproduce figures, tables, or portions of articles originally published in *Circulation* can be obtained via RightsLink, a service of the Copyright Clearance Center, not the Editorial Office. Once the online version of the published article for which permission is being requested is located, click Request Permissions in the middle column of the Web page under Services. Further information about this process is available in the [Permissions and Rights Question and Answer](#) document.

**Reprints:** Information about reprints can be found online at:  
<http://www.lww.com/reprints>

**Subscriptions:** Information about subscribing to *Circulation* is online at:  
<http://circ.ahajournals.org/subscriptions/>